HHS Public Access

Author manuscript

Nat Cell Biol. Author manuscript; available in PMC 2020 June 22.

Published in final edited form as:

Nat Cell Biol. 2019 December ; 21(12): 1590–1603. doi:10.1038/s41556-019-0415-1.

Translational Reprogramming Marks Adaptation to Asparagine Restriction in Cancer

Gaurav Pathria[1,*], **Joo Sang Lee**[2,3,9], **Erez Hasnis**[1,9], **Kristofferson Tandoc**[4], **David A. Scott**[1], **Sachin Verma**[1], **Yongmei Feng**[1], **Lionel Larue**[5,6,7], **Avinash D Sahu**[8], **Ivan Topisirovic**[3], **Eytan Ruppin**[2], **Ze'ev A. Ronai**[1,*]

[1]Tumor Initiation and Maintenance Program, Cancer Center, Sanford Burnham Prebys Medical Discovery Institute, La Jolla, CA 92037, USA

[2]Cancer Data Science Lab (CDSL), National Cancer Institute, National Institute of Health, Bethesda, MD 20892, USA

[3]Samsung Medical Center, Sungkyunkwan University School of Medicine, Suwon 16419, Republic of Korea

[4]Lady Davis Institute, SMBD Jewish General Hospital, Gerald Bronfman Department of Oncology, Departments of Experimental Medicine and Biochemistry, McGill University, Montreal, QC H3A 1A3, Canada

[5]Institut Curie, PSL Research University, INSERM U1021, Normal and Pathological Development of Melanocytes, Orsay, France

[6]Univ Paris-Sud, Univ Paris-Saclay, CNRS UMR 3347, Orsay, France

[7]Equipe Labellisée Ligue Contre le Cancer, Orsay, France

[8]Harvard School of Public Health & Massachusetts General Hospital, Boston 02115, USA

[9]Equal contribution

Abstract

While amino acid restriction remains an attractive strategy for cancer therapy, metabolic adaptations limit its effectiveness. Here we demonstrate a role of translational reprogramming in the survival of asparagine-restricted cancer cells. Asparagine limitation in melanoma and pancreatic cancer cells activates RTK-MAPK as part of a feedforward mechanism involving mTORC1-dependent increase in MNK1 and eIF4E, resulting in enhanced translation of *ATF4* mRNA. MAPK inhibition attenuates translational induction of ATF4 and the expression of its target asparagine biosynthesis enzyme ASNS, sensitizing melanoma and pancreatic tumors to

*Correspondence: zeev@ronailab.net (Z.A. Ronai); gpathria@sbpdiscovery.org (G. Pathria).

Author Contributions

GP and ZAR conceived the study; GP, EH, IT, ER, and ZAR designed experiments; GP, EH, KT, SV, and YF performed experiments; GP and DAS conducted metabolic analyses; LL provided valuable reagents; GP, JSL, ADS, EH, KT, ER, and ZAR analyzed data; and GP, ER, IT, and ZAR wrote the manuscript.

Competing Interests

ZR and ER are co-founders (divested) and serving as a non-paid scientific advisors to Pangea Therapeutics.

asparagine restriction, reflected in their growth inhibition. Correspondingly, low *ASNS* expression is among the top predictors of response to MAPK signaling inhibitors in melanoma patients and is associated with favorable prognosis, when combined with low MAPK signaling activity. While unveiling a previously unknown axis of adaptation to asparagine deprivation, these studies offer the rationale for clinical evaluation of MAPK inhibitors in combination with asparagine restriction approaches.

Keywords

Asparagine; MAPK; synthetic lethality; ATF4; GCN2; MNK1; mTORC1; L-asparaginase; translation

Introduction

Rapidly proliferating tumors exhibit increased requirement for macromolecules to meet expanding energetic and biosynthetic needs. Therefore, nutrient limitation is widely recognized as a potential therapeutic strategy. However, cancer cells successfully endure harsh, nutrient-restricted environments, often by rewiring metabolic pathways. Accordingly, *de novo* synthesis of non-essential amino acids has been demonstrated to impede durable therapeutic response[1,2].

While supporting enhanced protein synthesis in tumor cells and anti-oxidant defense through glutathione biosynthesis, glutamine anaplerotically fuels the tricarboxylic acid (TCA) cycle, thus generating ATP and precursors for nucleotide, amino acid, and lipid biosynthesis[3,4]. Cancer cells can sustain glutamine-dependent processes in the absence of exogenous glutamine through *de novo* glutamine biosynthesis, with the notable exception of asparagine biosynthesis[5,6]. Since the inability to maintain cellular asparagine levels underlie tumor growth suppression seen upon glutamine restriction, curtailing cellular asparagine levels is an appealing alternative to limit tumor growth[7,8].

Asparagine synthetase (ASNS) converts aspartate to asparagine, which is accompanied by glutamine deamidation. A deficiency of ASNS in acute lymphoblastic leukemia (ALL) renders ALL cells sensitive to asparagine restriction [9]. However, asparagine restriction approaches were ineffective in solid tumors that express low levels of ASNS[10-13]. Here we show that MAPK signaling supports translational reprogramming for the survival of asparagine-restricted tumors, providing the molecular basis for rational combinations which rely on asparagine restriction strategies.

Results

ATF4 Activity Impedes Growth-Suppression in Response to Asparagine Limitation

We first determined the effect of ASNS depletion on a panel of pancreatic, breast, prostate, and melanoma cell lines. *ASNS* suppression (*si-ASNS*) compromised proliferation in all cell lines tested relative to those treated with non-targeting (NT)-siRNA (Fig. 1a). Gas chromatography-mass spectrometric (GC-MS) analysis confirmed decrease in asparagine levels upon ASNS depletion (Extended Data Fig. 1a). si-*ASNS*-mediated suppression of

pancreatic cancer and melanoma cell proliferation was largely abolished when cultured in L-asparagine (L-Asn)-containing growth medium (Fig. 1b and Extended Data Fig. 1b). Conversely, addition of L-Asparaginase (L-A'ase) to the L-Asn-containing media impaired proliferation of si-*ASNS*-treated cells (Fig. 1b). Thus, suppressing *de novo* biosynthesis as well as compromising exogenous asparagine availability enables effective inhibition of cancer cell proliferation.

ASNS depletion in A375 and UACC-903 melanoma cells resulted in the activation of GCN2, which was accompanied by increased eIF2α phosphorylation, ATF4 protein levels and expression of its target genes, as compared to control cells (Fig. 1c and 1d), reflecting activation of the Amino Acid Response (AAR) pathway[14]. Importantly, activation of the GCN2-ATF4 axis following ASNS suppression was abrogated by the addition of L-Asn to the medium (Extended Data Fig. 1c) whereas depletion of L-Asn by L-A'ase reverted these effects (Fig. 1e).

Given that the activation of GCN2-ATF4 pathway serves as a therapeutic roadblock[15], we tested whether disruption of this axis may potentiate the effects of ASNS suppression. *GCN2* silencing blocked si-*ASNS*-induced ATF4 upregulation, whereby combination of si-*GCN2* and si-*ASNS* inhibited melanoma cell proliferation more effectively than either siRNA alone (Fig. 1f,g). Additionally, while attenuating the activation of ATF4 target genes, si-*ATF4* augmented the anti-proliferative effects of si-*ASNS* (Fig. 1h-j). Finally, suppression of ATF4 induction by Integrated Stress Response Inhibitor (ISRIB) potentiated anti-proliferative effects of ASNS depletion in melanoma cells (Extended Data Fig. 1d). These data demonstrate that the disruption of GCN2-ATF4 axis potentiates anti-proliferative effects of asparagine limitation (Fig. 1k)

Bioinformatics and Functional Analysis Identifies MAPK as a Synthetic Lethal Signaling Partner for ASNS

A bioinformatic pipeline that identifies clinically relevant Synthetic Lethal Interactions[16] (ISLE) (Fig. 2a) predicted seven synthetic lethal (SL) partners of ASNS (Supplementary Table 1). Those included RTKs (VEGFR-2, PDGFR-A, and PDGFR-B), the Mitogen-Activated Protein Kinase Kinase Kinase (MAP3K; BRAF) and MAP kinase-interacting serine/threonine protein kinase (MKNK1 or MNK1), an effector of MAPK signaling and a regulator of translation initiation[17]. Polo-like Kinase 1, a Ser/Thr kinase that activates MAPK signaling through CRAF phosphorylation[18] was also identified. Identification of multiple candidates that are part of, or affected by, the MAPK signaling axis suggested this pathway may provide synthetic vulnerability for low *ASNS*-expressing (*ASNS*^{lo}) tumors (Fig. 2b).

Notably, each of the identified SL partners significantly reduced the risk of cancer-related death when inactivated together with ASNS (Fig. 2c) and *ASNS* expression was one of the strongest predictors of response to the BRAF inhibitor AZ628 (Fig. 2d). *ASNS*^{lo} cell lines showed greater sensitivity to the pharmacological inhibitors of the predicted SL partners as compared to high *ASNS*-expressing (*ASNS*^{hi}) cell lines (Fig. 2e,f and Extended Data Fig. 2a). Furthermore, shRNA screens confirmed that ASNS SL partner genes exhibit higher essentiality in *ASNS*^{lo} cell lines. Likewise, greater essentiality for key MAPK pathway

components was seen in *ASNS*^{lo} as compared to *ASNS*^{hi} cells (Fig. 2g and Extended Data Fig. 2b). ATF4, shown to impede the anti-proliferative efficacy of asparagine restriction (Fig. 1j), also exhibited higher essentiality in *ASNS*^{lo} cells (Extended Data Fig. 2b).

BRAF inhibition alone suppressed melanoma cell proliferation, but its combination with *ASNS* knockdown was more effective (Fig. 3a). These observations were confirmed using additional BRAF (GDC-0879) or MEK (MAP Kinase Kinase; PD-325901 and CI-1040) inhibitors. Drug concentrations that inhibited melanoma cell proliferation by 40-60% were more effective (>80% inhibition) when combined with *ASNS* knockdown (Extended Data Fig. 3a). These findings confirm the synthetic lethality between MAPK signaling and ASNS.

As activation of the GCN2-ATF4 axis appears to be a major impediment to the efficacy of asparagine restriction[15] (Fig. 1), we assessed whether the synthetic lethal effects seen upon inhibition of MAPK signaling and *ASNS* knockdown are associated with the activation of this axis. To this end, melanoma cells were treated with pharmacological inhibitors for BRAF, MEK or ERK, or subjected to genetic inactivation of *BRAF* by RNAi. In all cases, inhibition of MAPK signaling attenuated ASNS depletion-dependent induction of the GCN2-ATF4 axis and the downstream targets (Fig. 3b-d and Extended Data Fig. 3b). Consistently, BRAF inhibition in melanoma cells attenuated transcriptional induction of ATF4 target genes seen following *ASNS* knockdown (Fig. 3e), resembling changes seen following ATF4 loss (Fig. 1i). Lastly, despite BRAF inhibition, ectopic expression of a constitutively active mutant of MEK1 (MEK1-CA; S218D, S222D) in A375 cells maintained ERK1/2 activity and abolished the ability of BRAF inhibition to block ATF4 induction in response to ASNS suppression (Fig 3f). Similarly, expression of MEK1-CA, but not MEK1-WT, effectively restored the proliferation of A375 cells that were subjected to si-*ASNS* and BRAF-i treatment (Fig. 3f). These observations substantiate the role of BRAF-MEK-ERK signaling axis in the induction of ATF4 and its associated survival signaling in response to ASNS suppression.

Notably, ASNS suppression also led to enhanced MEK and ERK phosphorylation, indicative of an undisclosed feedforward mechanism (Fig. 3b-d and Extended Data Fig. 3b). Accordingly, *ASNS* knockdown in melanoma cells increased levels of *FRA1*, *c-MYC*, *CCND1,* and *MMP9*, transcripts whose expression is positively regulated by MAPK signaling[19] (Extended Data Fig. 3c).

Similar to melanoma cells, *ASNS* knockdown in the pancreatic cancer cell lines, which harbor an activating KRAS mutation, induced MAPK signaling, ATF4 and ATF4 target PSAT1, changes that were alleviated upon MEK inhibition (Extended Data Fig. 3d). Furthermore, in si-*ASNS*-treated cancer cells, depletion of L-Asn in the culture medium by addition of L-A'ase enhanced ERK1/2 phosphorylation (Extended Data Fig. 3e). Conversely, supplementing the medium with L-asparagine prevented ERK phosphorylation in melanoma cell lines following ASNS suppression (Extended Data Fig. 3f), demonstrating the role of cellular asparagine in regulating MAPK signaling activity. Lastly, *ASNS* knockdown suppressed the proliferation of mutant RAS cancer cell lines, which was further attenuated when combined with MEK inhibition (Extended Data Fig. 3g). These findings

indicate that MAPK activity is required for the induction of ATF4 levels in diverse ASNS-depleted cancer cells.

As ATF4 target genes that encode serine/glycine (PSAT1) and alanine (GPT2) biosynthesis enzymes were induced following ASNS downregulation (Fig. 1d,i), we determined the levels of corresponding amino acids in *ASNS*-depleted *vs.* non-depleted UACC-903 melanoma cells. Consistent with upregulation of PSAT1 and GPT2 expression, ASNS suppression was accompanied by increased cellular levels of serine, glycine and alanine (Extended Data Fig. 3h), compared with control cells. In addition to the induction of serine, glycine, and the one-carbon (SGOC) metabolic network enzyme PSAT1 (Fig. 1 and 3), *ASNS* knockdown also induced expression of other enzymes in this metabolic network (i.e., Phosphoglycerate Dehydrogenase (*PHGDH*), Phosphoserine Phosphatase (*PSPH*), and Serine Hydroxymethyltransferase 1 (*SHMT1*), an effect largely abolished upon BRAF inhibition (Extended Data Fig. 3i). In agreement, GC-MS-based analysis of the *ASNS*-silenced UACC-903 cells showed that elevated intracellular levels of serine, glycine, and alanine were reversed by BRAF or MEK inhibition (Fig. 3g). Likewise, isotope ([$^{13}C_6$]-Glucose)-tracing confirmed increased incorporation of glucose-derived carbons in serine and glycine following ASNS suppression, which was blocked by BRAF inhibition, underscoring the underlying enhancement in *de novo* serine/glycine biosynthesis (Extended Data Fig. 3j). Intriguingly, intracellular lactate levels also increased in UACC-903 cells following *ASNS* knockdown and were reversed by BRAF or MEK inhibition (Fig. 3g). These changes can be attributed to increased lactate-generating enzyme lactate dehydrogenase A (LDHA) expression, a target for MAPK signaling-regulated c-MYC[20]. Indeed, consistent with upregulation of *c-MYC* (Extended Data Fig. 3c), *ASNS* knockdown increased, while BRAF inhibitor suppressed *LDHA* expression (Extended Data Fig. 3k).

Consistent with the idea that downregulation of an SL pair results in tumor growth inhibition, a more favorable prognosis was observed in patients with a concomitant downregulation of *ASNS* and *BRAF* (used as proxy for MAPK signaling axis) (Fig. 3h). Collectively, these findings suggest that MAPK signaling activity is central for the induction of ATF4 and related phenotypic and metabolic changes following ASNS suppression (Fig. 3i).

MAPK Signaling-Dependent Translational Reprogramming Promotes *ATF4* mRNA Translation

The identification of MNK1, a protein implicated in the control of translation initiation[17] as a SL partner of ASNS led us to assess the importance of mRNA translation machinery in cellular adaptation to ASNS suppression. ERK1/2 promotes mTORC1 activity by suppressing the activity of its negative regulator Tuberous Sclerosis 2 (TSC2)[21]. *ASNS* depletion in melanoma cells led to inhibition of TSC2 phosphorylation, with a concomitant mTORC1 activation (Fig. 4a). Corresponding increase in the phosphorylation of TSC2 and mTORC1 substrates, including eIF4E-Binding Protein (4E-BP1), p70 Ribosomal S6 Kinase (p70S6K), and its substrate ribosomal protein S6 (rpS6/S6) was abrogated by BRAF inhibition (Fig. 4a). Similarly, *BRAF* knockdown or ERK inhibition compromised enhanced mTORC1 activity in melanoma and pancreatic cancer cell lines treated with si-*ASNS*

(Extended Data Fig. 4a,b,c). While these data suggest that blocking MAPK signaling may increase intracellular levels of free amino acids, inhibition of BRAF or MEK failed to rescue asparagine levels in ASNS depleted cells (Fig. 4b). This implies that attenuated ATF4 induction by MAPK signaling inhibition (Fig. 3) is not due to the restoration of free cellular asparagine.

mTORC1 stimulates protein synthesis, in part, via phosphorylation and inactivation of 4E-BPs, which suppress mRNA translation by sequestering the mRNA 5' cap-binding protein eIF4E[22]. Thus, we assessed whether MAPK-dependent mTORC1 activation, seen upon ASNS depletion, promotes ATF4 induction in eIF4E-dependent manner. *eIF4E* depletion in melanoma cells blocked the induction of ATF4 and its transcriptional targets seen upon ASNS suppression (Fig. 4c,d). Similarly, treatment with either allosteric (rapamycin) or active-site (torin 1) mTOR inhibitors of *ASNS* knocked-down melanoma and pancreatic cancer cell lines blocked the induction of ATF4 and its targets (Fig. 4e-g and Extended Data Fig. 4d,e). Importantly, inhibition of either MAPK or mTORC1 failed to attenuate the basal expression of S6, 4E-BP1, or ERK1/2 (Fig. 4e,f and Extended Data Fig. 4a-e), pointing to differential requirement of mTORC1 activity for ATF4 translation, in response to asparagine limitation.

To confirm that altered ATF4 protein levels, seen upon ASNS suppression and/or MAPK inhibition, occurs at the level of translation, we performed polysome profiling[23] in A375 melanoma cells treated with either si-*ASNS*, BRAF inhibitor, or combination thereof. In comparison to mock-treated cells, ASNS suppression increased *ATF4* mRNA translation as illustrated by the shift of *ATF4* mRNA from subpolysomal (fractions 6-8) to heavy polysome (fractions 12-16) fractions, while BRAF inhibition caused the opposite effect (Fig. 4h). Importantly, BRAF inhibition attenuated the increase in translational efficiency of *ATF4* mRNA caused by ASNS depletion, as evidenced by lower *ATF4* mRNA levels in the heavy polysome fractions and concomitant increase in sub-polysomal fractions as compared to *ASNS* depletion alone (Fig. 4h). mTORC1 inhibition enhanced the anti-proliferative activity of *ASNS* knockdown in various cancer cell lines (Fig. 4i and Extended Data Fig. 4f), further supporting the role of MAPK-mTORC1-eIF4E axis. Lastly, *TSC2* knockdown in *ASNS* silenced cells, which uncoupled mTORC1 activity from MAPK signaling, resulted in a partial rescue of mTORC1 activity, ATF4 induction and its target gene (PSAT1 and GPT2) expression, despite BRAF inhibition (Fig. 4j). Altogether, these data point to the importance of MAPK-mTORC1-eIF4E signaling for translational reprogramming in ASNS-depleted cells, which enhances translation of *ATF4* mRNA (Fig. 4k).

MNK1 modulates translation by its direct phosphorylation of eIF4E (Ser-209 in mammals)[24], enhancing the latter's oncogenic potential[25,26]. Notably, *MNK1* knockdown in melanoma cells compromised ATF4 induction and almost completely ablated ATF4-mediated transcriptional changes seen upon ASNS suppression (Fig. 5a,b and Extended Data Fig. 5a). CRISPR-Cas9-mediated inactivation of MNK1 in ASNS-depleted A375 cells suppressed the increase in ATF4 protein, compared to MNK1-expressing cells (Fig. 5c). Polysome profiling of A375 melanoma cells co-depleted of ASNS and MNK1 showed lower degree of *ATF4* mRNA translation, compared with ASNS-only depleted cells (Fig. 5d).

Together, these data demonstrate that MNK1 is required for enhanced *ATF4* mRNA translation following ASNS suppression.

MNK1 knockdown in melanoma cells did not alter si-*ASNS*-dependent increases in mTORC1 activity (Fig. 5a), implying that MNK1 regulation of ATF4 occurs independent of changes in mTORC1. *MNK1* knockdown in pancreatic cancer cell lines also blocked ATF4 induction following *ASNS* knockdown, suggesting a general requirement for MNK1 in translation reprogramming in response to asparagine restriction (Extended Data Fig. 5b). Consistently, *MNK1* knockdown potentiated the anti-proliferative effects of *ASNS* knockdown (Extended Data Fig. 5c). Notably, pan-tumor analysis showed that low expression of both *ASNS* and *MNK1* in patient tumors is associated with better survival, highlighting co-targeting of ASNS and MNK1 as a possible therapeutic strategy (Fig. 5e).

Activation of MAPK signaling was shown to promote MNK1 phosphorylation[27]. Enhanced MAPK signaling in melanoma cells subjected to *ASNS* knockdown (Fig. 3) also increased MNK1 protein, albeit, with minimal changes in its transcript levels (Fig. 5f and Extended Data Fig. 5d). Similarly, L-A'ase treatment of melanoma cells subjected to *ASNS* knockdown and cultured in L-Asn-containing medium increased levels of phosphorylated and total MNK1 protein (Extended Data Fig. 5e). These observations suggested that MAPK/mTORC1 activity may increase *MNK1* mRNA translation. Indeed, ASNS suppression in A375 cells increased translation of *MNK1* mRNA (Fig. 5g).

Phosphorylation of eIF4E Ser-209 has been associated with MNK1-mediated translational regulation[28]. *ASNS* knockdown in melanoma cells increased phospho-(S209)-eIF4E and total eIF4E protein, but not the corresponding transcript levels (Fig. 5f and Extended Data Fig. 5f), pointing to enhanced translation of *eIF4E* mRNA as part of translational reprogramming seen in response to *ASNS* suppression. Consistently, ASNS suppression increased the translation of *eIF4E* mRNA (Fig. 5g). Importantly, no such change for histone *H3A* mRNA, while a decrease in *E-cadherin* (*CDH1*) mRNA was seen in heavy polysomal fractions (Extended Data Fig. 5g), pointing to selective changes in mRNA translation following ASNS suppression. Interestingly, *MNK1* knockdown in melanoma cells did not suppress eIF4E Ser-209 phosphorylation, while blocking ATF4 induction (Fig. 5f). Treatment of A375 cells with the MNK1 inhibitor eFT508, did not antagonize ATF4 induction upon ASNS suppression (Extended Data Fig. 5h), implying that additional regulatory components may contribute to MNK1 effect on *ATF4* mRNA translation. Inhibition of BRAF, ERK, or mTORC1 in melanoma cells blocked increase in the levels of phosphorylated and total MNK1 and eIF4E protein seen following ASNS suppression (Fig. 5h and Extended Data Fig. 5i,j). Lastly, increased translation of *MNK1* and *eIF4E* mRNAs following ASNS suppression (Fig. 5g) was impeded by BRAF inhibitors (Fig. 5i). These data implicate MAPK signaling in translational reprogramming in response to asparagine limitation via regulation of mTORC1, with concomitant effect on MNK1 and eIF4E expression and activity (Fig. 5j).

Enhanced MAPK Pathway Activity Following Asparagine Limitation is RTK Signaling Dependent

EGFR is an upstream modulator of MAPK signaling and its transcript carries an Internal Ribosome Entry Site (IRES)[29]. We thus asked whether enhanced MAPK pathway activity following ASNS suppression may be mediated by EGFR. si-*ASNS* treatment of melanoma cells did not increase *EGFR* mRNA expression but enhanced EGFR protein levels, independent of mTORC1, eIF4E or MNK1 activity, pointing to IRES-mediated[29] cap-independent and/or eIF3d-mediated cap-dependent translation[30,31] (Extended Data Fig. 6a-e). Notably, treatment of melanoma cells with the EGFR inhibitor gefitinib did not alter ERK1/2 activation following *ASNS* knockdown (Extended Data Fig. 6f), suggesting that either a different mechanism(s) may compensate for EGFR inhibition, or that EGFR may be dispensable for MAPK activation under limiting asparagine conditions. Given that RTKs are upstream of MAPK signaling and ISLE analysis predicted VEGFR-2, PDGFR-A, and PDGFR-B as synthetic lethal partners of ASNS (Fig. 2), we monitored possible changes in the expression of these RTKs following ASNS suppression. While *VEGFR-2* transcript levels increased in melanoma cells following ASNS suppression, *PDGFR-A* and *PDGFR-B* transcript levels did not (Fig. 6a and Extended Data Fig. 6g). Yet, increased protein levels of VEGFR-2 and PDGFR-B were seen in both melanoma cell lines following ASNS suppression, while PDGFR-A was only induced in UACC-903 cells (Fig. 6b). Enhanced translation of *VEGFR-2* and *PDGFR-B* mRNA was confirmed in polysome profiling of A375 cells subjected to ASNS suppression (Fig. 6c). Possible changes in the translation of these RTKs were further monitored using L-azidohomoalanine (AHA), a methionine analog which incorporates into newly synthesized proteins[32]. ASNS suppression in melanoma cells resulted in increased AHA incorporation into newly synthesized VEGFR-2 and PDGFR-B, but not α-Tubulin or GAPDH (Extended Data Fig. 6h), providing independent support for enhanced translation of *VEGFR-2* and *PDGFR-B* mRNA. Treatment of ASNS-depleted melanoma cells with ISRIB (Extended Data Fig. 6i), or *GCN2* silencing (Extended Data Fig. 6j) alleviated the induction of VEGFR-2 and PDGFR-B, further supporting the role of translational reprogramming in their upregulation.

To determine whether enhanced RTK signaling was required for MAPK pathway activation upon ASNS suppression, we tested the effect of Sunitinib, a small-molecule inhibitor of multiple RTKs. Sunitinib antagonized enhanced phosphorylation of both MEK1/2 and ERK1/2 and also mitigated ATF4 upregulation in ASNS-depleted melanoma cells (Fig. 6d), consistent with the requirement of MAPK signaling for induction of ATF4. Among the 3 RTKs, *VEGFR-2* knockdown was more effective in both melanoma cell lines subjected to ASNS depletion, as it almost completely ablated ATF4 induction (Fig. 6e) and attenuated the enhanced expression of ATF4 target genes (Fig. 6f). These studies identify RTK activity as an upstream regulator of MAPK signaling and the ensuing ATF4 induction following ASNS suppression (Fig. 6g).

Inhibition of Melanoma and Pancreatic Tumor Growth *In Vivo* by Combined Asparagine Restriction and MAPK Signaling Inhibition

Comparing the expression of *ASNS* in tumor samples of different cancer types *vs.* healthy donors revealed that *ASNS* is down-regulated in multiple cancer types compared to the

corresponding healthy tissues, including melanoma and pancreatic cancer (Extended Data Fig. 7a), marking these cancers as potential candidates for L-A'ase therapy. Our data demonstrating that concomitant MAPK inhibition renders cancer cells incapable of upregulating ATF4 and its transcriptional target ASNS, provided the rationale to assess the growth inhibitory potential of combined MAPK signaling inhibition and L-A'ase. Indeed, treatment of melanoma and pancreatic cancer cell lines with MEK-i and L-A'ase, resulted in a markedly greater suppression in proliferation, compared to either treatment alone (Extended Data Fig. 7b). *In vivo*, the effect of combined L-A'ase and MEK-i treatment was assessed using the orthotopic KPC/B6 pancreatic cancer model. While L-A'ase treatment led to a significant inhibition of tumor growth, MEK-i treatment did not (Fig. 7a). Importantly, combination of L-A'ase with MEK-i (at a dose ineffective on its own) enhanced the suppression of pancreatic tumor growth (Fig. 7a). Resected tumors exhibited a markedly greater suppression in tumor cell proliferation as compared to either treatment alone (Fig. 7b,c). Notably, although MEK-i treatment alone did not result in a significant increase in apoptosis, it greatly augmented the ability of L-A'ase to promote apoptotic cell death (Fig. 7b,d). Further molecular analysis of the resected tumors from the L-A'ase treatment group revealed upregulation of ATF4 and ASNS protein levels, together with increased phosphorylation of ERK1/2, in comparison to the vehicle treatment group (Fig. 7e,f). Increased ATF4 protein levels in L-A'ase treated tumors also correlated with enhanced transcript levels of ATF4 target genes, including *ASNS*, compared with tumors from vehicle-treated animals (Fig. 7g). Importantly, combination of MEK inhibition and L-A'ase treatment *in vivo* overcame the increase in ERK1/2 phosphorylation and abolished the increase in ATF4 and the expression of its target genes, including ASNS (Fig. 7e-g).

In vivo assessment of the L-A'ase and MEK-i combination on melanoma growth was performed using an NRAS mutant melanoma (MaNRAS1)[33], in an immune-competent mouse model. Unlike the effect seen in pancreatic tumors, L-A'ase treatment did not exert a significant impairment of melanoma tumor growth, while administration of MEK-i had a modest anti-tumor activity (Fig. 7h). Yet, the combined treatment with L-A'ase and MEK-i led to a more robust tumor growth suppression compared with either treatment alone (Fig. 7h). Molecular analysis of the resected tumors confirmed induction of phosphorylated ERK1/2, ATF4, and of ASNS protein levels in response to L-A'ase treatment, which were reversed upon concurrent MEK-i treatment (Fig. 7i). Immunohistological analyses of tumor tissues revealed diminished proliferation in the combination group, compared with individual L-A'ase or MEK-i treatment groups (Fig. 7j,k). Similar to what was observed in pancreatic tumors, the combination of MEK-i and L-A'ase resulted in increased apoptosis in comparison to their individual treatment (Fig. 7j,l). Lastly, to study the possible effect of L-A'ase plus MEK-i on melanoma metastasis, we turned to NRAS mutant SW1 melanoma cells that metastasize to lungs in a syngeneic C3H/HeN mice[34]. While L-A'ase didn't exhibit a significant impairment of tumor growth, MEK-i showed a weak anti-tumorigenic activity, in comparison to vehicle-treated cells (Extended Data Fig. 7c). Importantly, L-A'ase and MEK-i combination effectively suppressed tumor growth, in a dose dependent manner, in comparison to either treatment alone (Extended Data Fig. 7c). Interestingly, L-A'ase treatment promoted lung metastasis (Fig. 7m), an effect reminiscent of enhanced lung metastasis observed in B16 melanoma cells deprived of glutamine, an essential precursor for

asparagine biosynthesis[35]. Significantly, while MEK-i showed some degree of anti-metastatic activity, when combined with L-A'ase a marked suppression of lung metastasis was observed, compared with either treatment alone (Fig. 7m). Notably, L-A'ase and MEK-i combination did not impact animal health, based on weight and liver enzyme profile. These findings substantiate the effectiveness of L-A'ase and MEK-i combination in suppressing melanoma and pancreatic cancer growth and melanoma metastasis.

Low ASNS Expression and MAPK Activity Correlates with Favorable Patient Prognosis

To substantiate our observations with ISLE and *in vivo* melanoma and pancreatic tumor studies, we analyzed RNA-Seq data that was obtained from 15 melanoma patients prior to their treatment with BRAF-i or a combination of BRAF-i and MEK-i. A significantly lower level of *ASNS* expression was identified in responders (>30% reduction in tumor size) *vs.* non-responders (<30% reduction in tumor size)[36] (Fig. 7n). Furthermore, *ASNS* was amongst the top 7 genes, whose expression was the strongest predictor of response to MAPK signaling inhibitors (Fig. 7o and Supplementary Table 2). Further, Receiver-Operating Characteristics (ROC) analysis in two independent cohorts of melanoma patients[36,37] identified *ASNS* expression as highly predictive of response to MAPK inhibition therapy (Fig. 7p,q).

Further analysis was performed on RNA-Seq data from two independent cohorts of paired (pre- and post-treatment) tumor specimens that were obtained from patients with metastatic melanoma, that were subjected to either BRAF-i or BRAF-i plus MEK-i treatment[37-39]. Since these cohorts consisted of tumors that exhibited resistance to these therapies, a possible correlation between ASNS expression and such resistance was assessed. Remarkably, development of resistance to MAPK pathway inhibition –monitored using post-treatment specimens– was associated with a significant increase in *ASNS* expression, compared with pre-treatment specimens (Fig. 7r,s). Together, these analyses provide important clinical evidence for the inverse relationship between ASNS expression and responsiveness to MAPK signaling inhibitors.

Discussion

Here we unveil a previously unknown role of MAPK signaling in translational reprogramming, which ensues in response to asparagine limitation, resulting in enhanced synthesis of the master stress response regulator ATF4, in melanoma and pancreatic cancer cells. While providing mechanistic understanding for the synthetic lethal interaction predicted between asparagine restriction and MAPK pathway inhibitors, our findings propose a therapeutic modality in solid tumors harboring low expression of ASNS[12].

Amino acid restriction results in translational reprogramming, which promotes translation of ATF4, among select uORF-containing mRNAs[40]. Our studies add additional important layers to this regulatory axis, as we demonstrate (i) the activation of the RTK-MAPK signaling following asparagine restriction (ii) the impact of this activation on the translation initiation regulators (mTORC1, MNK1, and eIF4E), which enhance the translation of *ATF4* mRNA, and (iii) the presence of a feedforward signaling axis, whereby translational reprogramming not only enhances ATF4 levels, but also of select RTKs, which further

enhance MAPK signaling to sustain translational reprogramming. Further, we demonstrate that under prolonged ASNS suppression, mTORC1 activity is not only maintained, but even enhanced, which at least in part can be attributed to MAPK-mediated TSC2 inhibition, adding an important perspective to an earlier study[41]. MAPK-mediated enhanced translation of *ATF4* mRNA, which in turn induces the expression of multiple amino acid transporters to enhance the uptake of essential amino acids, may also underlie the increase in mTORC1 activity[42-44]. Notably, MAPK-dependent translational reprogramming, which enhances ATF4 levels, explains previous observations, whereby ATF4 induction in response to glucose or histidine restriction was attenuated by MAPK signaling inhibitors[45,46].

While our studies have demonstrated the role of ATF4, a possible role of ATF6, XBP1[47] and ATF5[48], effectors of ER stress and mitochondrial UPR respectively, remains to be explored. ATF4 regulated genes include members of the hypoxia response (VEGFA)[49] and those implicated in programmed cell death (ATF3)[50]. Likewise, the activation of MAPK following asparagine restriction could induce hypoxia-inducible factor-1α (HIF-1α)[51], influencing metabolic rewiring and metastatic programs. It is therefore plausible that synthetic lethality induced upon combination of L-A'ase and MEK-i may impact ATF3 and HIF-1α signaling, as part of broader ATF4 transcriptional network.

Although we document the requirement of the GCN2-eIF2α axis for increased mRNA translation of select RTKs following ASNS suppression, the precise mechanism underlying this regulation remains to be established. Selective translation of transcripts that contain uORF elements, as present in *VEGFR-2* and *PDGFR-B* mRNA[52], may be attributed to the integrated stress response (ISR)[30], although additional regulatory cues, triggered upon asparagine limitation may also play a role. Furthermore, although almost 45% of 5'UTRs harbor at least one uORF[53,54], only a small number of mRNAs containing uORF elements have been shown to regulate the expression of downstream coding sequences upon eIF2α phosphorylation[55]. Further dedicated efforts will help establish the detailed mechanistic basis and the potential role of uORFs in the translational induction of VEGFR-2 and PDGFR-B.

While failing to ablate mTORC1 activity, limiting availability of a single amino acid (asparagine) promotes undesired activation of MAPK signaling, thereby signifying acquisition of new capabilities by cancer cells. As MAPK signaling promotes invasive and metastatic phenotypes[56], through distinct underlying mechanisms, including modulation of HIF-1α[51], this finding may explain enhanced metastatic potential of cancer cells, seen in response to glutamine deprivation[35], consistent with our observation of increased melanoma lung metastasis upon L-A'ase treatment. Thus, impairment of both proliferative and invasive phenotypes is expected to provide a therapeutic benefit, which can be achieved by combining asparagine restriction and MAPK pathway inhibition.

While providing an explanation for the lack of clinical efficacy of L-A'ase in pancreatic cancer and melanoma patients[11,13], our finding that MAPK inhibitors reprogram translation to attenuate induction of ATF4 and its target ASNS, offers a therapeutic modality relying on L-A'ase combination with MAPK pathway inhibitors.

Overall, our studies demonstrate that adaptation to asparagine limitation is MAPK signaling and consequent translational reprogramming dependent, thus providing the rationale for clinical evaluation of co-targeting MAPK and asparagine metabolism pathways for cancer therapy.

Methods

Cell Culture and Reagents

Cancer cell lines (pancreatic, Mia-Paca-2, Panc-1 and BX-PC3; breast, MDA-231 and MCF7; prostate, PC-3 and LNCaP; and melanoma, A375, and Sk-Mel28) were obtained from ATCC. WM-35 and WM1366 melanoma cell lines were a kind gift from Meenhard Herlyn (Wistar Institute) and UACC-903 melanoma cell line was obtained from the University of Arizona Cancer Center. All cell lines were cultured in Dulbecco's modified Eagle's medium (DMEM; GE Healthcare Life Sciences, IL, USA), supplemented with 5% fetal bovine serum and penicillin–streptomycin. MaNRAS1 (1007) mouse melanoma cell lines were established in culture from C57BL/6 Tyr::NRAS^{Q61K} male and female transgenic animals, respectively[57] (Petit et al., in preparation). Cells were maintained in Ham's F12 medium (Gibco) supplemented with 10% decomplemented fetal bovine serum Sigma-Aldrich (St. Louis, MO), 5 mM L-glutamine, 100U/mL penicillin and 100μg/mL streptomycin. All cells were grown at 37°C in a humidified atmosphere containing 5% carbon dioxide. All cells were incubated at 37°C. L-Glutamine-$^{13}C_5$, D-Glucose-$^{13}C_6$, and L-asparagine was purchased from Sigma-Aldrich. PLX-4032 (used at 200 nM), GDC-0879 (used at 250 nM), CI-1040 (used at 500 nM), SCH-772984 (used at 250 nM), Torin 1 (used at 100 nM), rapamycin (used at 100 nM), gefitinib (used at 1μM), sunitinib (used at 500 nM) (Selleckchem, Houston, TX), PD-325901 (used at 250 nM) (LC laboratories, Woburn, MA), ISRIB (used at 200 nM) (Tocris, Minneapolis, MN), eFT508 (used at 100 nM) (Effector Therapeutics, San Diego, CA). L-asparaginase was purchased from Prospec Protein Specialists (Rehevot, Israel). Wild-type (WT) MEK1-pcw107-V5 and constitutively active (CA) MEK1 (S218D, S222D)-pcw107 were purchased from Addgene (Watertown, MA). For CRISPR-mediated inhibition of MNK1 expression, A375 cells stably expressing Cas9 (Lenti-Cas9-2A-Blast, Addgene plasmid #73310) were transduced with lentivirus expressing MNK1 sgRNAs (Sigma-Aldrich, Clones: HS5000002615; HS5000002616) and selected with puromycin for 2–3 days. Single clones were expanded and screened by protein immunoblot. The sgRNA sequences used were AAGCTGTTTGAAAGCATCCAGG and GAGTTTCCTGACAAGGACTGGG. For all experiments, measurements were taken from independent samples.

Antibodies

The following antibodies were used: ATF4 (D4B8) (dilution, 1:1,000) (Cat#11815), MNK1 (C4C1) (dilution, 1:1000) (Cat#2195), phospho-MNK1 (dilution, 1:1,000) (Thr197/202) (Cat#2111), phospho-eIF4E (S209) (dilution, 1:1,000) (Cat#9741), eIF4E (dilution, 1:1,000) (Cat#9742), EGFR (D38B1) (dilution, 1:1,000) (Cat#4267), SLC1A5 (ASCT2, V501) (dilution, 1:1,000) (Cat#5345), phospho(Ser235/236)-S6 Ribosomal Protein (D68F8) (dilution, 1:1,000) (Cat#4858), S6 Ribosomal Protein (54D2) (dilution, 1:1,000) (Cat#2217), phospho(Thr37/46)-4E-BP1 (236B4) (dilution, 1:1,000) (Cat#9451), 4E-BP1 (dilution,

1:1,000) (Cat#9452), GCN2 (dilution, 1:1,000) (Cat#3302), phospho(Ser51)-eIF2α (dilution, 1:1,000) (Cat#9721), eIF2α (dilution, 1:1,000) (Cat#9722), phospho-p44/42 Erk1/2 (Thr202/Tyr204) (dilution, 1:1,000) (Cat#9101), p44/42 Erk1/2 (dilution, 1:1,000) (Cat#9102), phospho-MEK1/2 (Ser217/221) (dilution, 1:1,000) (Cat#9121), MEK1/2 (dilution, 1:1,000) (Cat#9122), VEGFR-2 (55B11) (dilution, 1:1,000) (Cat#2479), PDGFR-A (D1E1E) (dilution, 1:1,000) (Cat#3174), PDGFR-B (28E1) (1:1,000) (Cat#3169), α-tubulin (1:5,000) (Cat#2144) and HRP-conjugated anti-Mouse (dilution 1:10,000) (Cat#7076) and HRP-conjugated anti-Rabbit (dilution, 1:10,000) (Cat#7074) antibodies from Cell Signaling Technology (MA, USA). Phospho-GCN2 (Thr-899) (dilution, 1:1,000) (Cat#ab75836) from Abcam (Cambridge, MA). PSAT1 (dilution, 1:1,000) (Cat#PA5-22124), anti-V5 (dilution, 1:1,000) (Cat#R960-25) from Thermo-Fisher Scientific (CA, USA). BRAF (F-7) (dilution, 1:250) (Cat#sc-5284), GPT2 (G-7) (dilution, 1:250) (Cat#sc-398383), ASNS (G-10) (dilution, 1:250) (Cat#sc-365809), HSP90 (F-8) (dilution, 1:5,000) (Cat#sc-13119), GAPDH (0411) (dilution 1:1,000) (Cat#sc-47724) from Santa Cruz Biotechnology, (TX, USA).

siRNA Transfection

$1x10^5$ cells were seeded overnight (O/N) per well in 6-well plates. Negative control (NT-siRNA) or si-RNA targeting the transcript of interest was transfected utilizing jetPRIME® transfection reagent, as per manufacturer's instructions (Polyplus, NY, USA). Following siRNAs were used: si-*ASNS*#1 (SASI_Hs01_00116724), si-*ASNS*#2 (SASI_Hs01_00116721), si-*ASNS*#3 (SASI_Hs01_00116722), si-*ATF4* (SASI_Hs02_00332313), si-*eIF4E* (SASI_Hs01_00216117), si-*BRAF* (SASI_Hs01_00107705), si-*GCN2* (SASI_Hs01_00097888), si-*MNK*#1 (SASI_Hs01_00228422), si-*MNK1*#2 (SASI_Hs01_00228423), si-*MNK1*#3 (SASI_Hs01_00228424), si-*VEGFR-2* (SASI_Hs01_00073461), si-*PDGFR-A* (SASI_Hs02_00341109), si-*PDGFR-B* (SASI_Hs01_00241713) and the negative control si-RNA (NT-siRNA; SIC001) were purchased from Sigma-Aldrich.

Immunoblotting

1-$2x10^5$ cells were seeded O/N per well in 6-well plates. Following treatment for the specified duration, total protein was extracted in Laemmli buffer, fractionated by SDS polyacrylamide gels and transferred to PVDF membranes (Millipore Sigma, MA, USA). After blocking with 5% non-fat dry milk (BD Biosciences, CA, USA), the membranes were incubated with primary antibodies overnight at 4 °C. Afterwards, 2 hr incubation with HRP-conjugated secondary antibodies was performed. Following chemiluminescence reaction, the protein signal was visualized using the ChemiDoc imaging system (Bio-Rad, Hercules, CA) according to the manufacturer's instructions.

Cell Proliferation

For cell proliferation, 0.3-$0.5x10^5$ cells were seeded O/N in triplicate in 6-well plate. Following treatment for the specified duration, cells were trypsinized and the cell count was determined with Neubauer hemocytometer (Celeromics, Cambridge, UK).

qPCR Analysis

$1x10^5$ cells were seeded O/N per well in 6-well plates. Following treatment for 48 hr, total RNA was extracted using RNeasy Mini Kit (Qiagen, Hilden, Germany). cDNA was synthesized using oligo(dT) and random primers (AB Bioscience, MA, USA), and qPCR analysis was performed with SYBR Green (Roche, NJ, USA). Primers were designed using the PrimerQuest tool (Integrated DNA Technologies, CA, USA) and Primer Bank (https://pga.mgh.harvard.edu/primerbank/). β-Actin was used as an internal control. List of primers and the corresponding sequences are shown in Supplementary Table 3.

13-C Metabolite Labeling and Amino Acid Quantification

Cell extraction and GC-MS analysis for metabolite quantification and $^{13}C_6$-glucose labeling determination were performed as described in Ratnikov et. al.[58]. The input label was 50% 13C-Glc or 13C-Gln. For GC-MS analysis, intracellular metabolite amounts are expressed as concentration (in nmol) per cell sample (cells from one well of six-well plates; approximately 0.5×10^6 to 1.0×10^6 cells).

AHA Labeling Assay

For labeling newly synthesized proteins, A375 and UACC-903 cells transfected with NT-siRNA control or si-*ASNS* for 48 hr were maintained in cysteine and methionine free DMEM for 1 hr, followed by growth in DMEM containing 100 mg/mL methionine or AHA (l-azidohomoalanine) (Thermo-Fisher Scientific) for 2 hr, as described previously[32]. Click reactions were performed using Click Chemistry Reaction Buffer Kit (Click Chemistry Tools) on cell extracts by incubation with 40 mM Biotin-PEG4-Alkyne for 30 min following the manufacturer's protocol. The resulting extracts were then used to pull-down biotin-labeled proteins using biotin binding Dynabeads (Thermo-Fisher Scientific), followed by measurement of newly synthesized VEGFR-2, PDGFR-B, α-Tubulin, and GAPDH proteins by immunoblotting using respective antibodies.

Conditional Gene Essentiality

Three large-scale shRNA single gene knockout screens[59-61] were analyzed. The essentiality of the genes of interest in $ASNS^{hi}$ vs. $ASNS^{lo}$ cell lines (partitioned by median gene expression value) was assessed using Wilcoxon rank sum test.

Kaplan Meier analysis

For Kaplan-Meier analysis of TCGA data, we used UCSC Xena browser (https://xena.ucsc.edu), encompassing 9,492 samples in 33 cancer types. A gene is termed underexpressed when its expression level is below bottom tertile across samples in the given cancer type. We considered co-underexpression of ASNS and BRAF/MKNK1, and the remainder of the samples as control. We compared the patient survival of the two groups using (two-sided) logrank test, and effect size was quantified with the difference in the area under the two Kaplan Meier curves (ΔAUC).

Differential Gene Expression Analysis

For the comparison to healthy tissues, we used the data from UCSC Xena browser (http://xena.ucsc.edu), where they normalized the TCGA samples with the 4,723 GTEx healthy tissue samples with exactly same platform which enables proper comparison. We compared the expression of ASNS in these cancer vs. healthy tissue samples using Wilcoxon rank sum test.

Patient Therapeutic Response

We analyzed two melanoma cohorts treated with MAPK inhibitors: (i) One cohort with BRAF-i or BRAF-i+MEK-i treatment (n=15, 8 patients treated with dabrafenib, 3 patients treated with vemurafenib, and 4 patients treated with dabtrafenib+trametinib)[36] and (ii) another cohort with BRAF-i treatment (n=23, dabtrafenib or vemurafenib)[37]. For the first cohort, response was determined based on RECIST tumor reduction (responder >30% reduction, non-responder <30% reduction). Effect size was determined by the difference in the median ASNS expression of responders vs non-responders. ROC analysis was performed to evaluate the performance of ASNS expression in predicting the responders. For the second cohort[37], the information of tumor size reduction was not available for many patients, so we considered RECIST criteria annotated as “RES” as responders and all other patients as nonresponders.

Synthetic Lethal Interaction Identification (ISLE)

ISLE was used to identify the synthetic lethal (SL) partners of ASNS in patients’ tumor as described in[16], with a slight modification to prioritize those candidates that have evidence in pharmacological functional screens. ISLE proceeds in the following two steps: (1) ISLE first identified putative SL partners of ASNS by mining both large-scale *in vitro* single drug response[62] and gene knock-down[59-61] datasets. The hypothesis is that the pharmacological inhibition or gene knockdown of a truly causal SL partner of ASNS will selectively inhibit the growth of cells lines where ASNS is downregulated. The two pancancer gene knock-down datasets were combined via Z-score transformation[60,61]. An *in vitro* drug response dataset consisting of the efficacies of 221 drugs across 628 cancer cell lines[62] was used to tease out such dependencies, where the cell lines with the bottom 10-percentile of ASNS expression or SCNA were denoted as $ASNS^{lo}$ as defined previously[63]. AZ628 was selected due to its strong effect size and significance in gene expression data, and additional candidates that were supported by both gene expression and SCNA data were selected. (2) It identifies, among the candidate pairs emerging from the first step, those interactions that are clinically relevant using patients’ mRNA expression (RNA-seq) and somatic copy number alterations (SCNA) data from TCGA, which covers 8,749 patient samples across 28 cancer types and integrates clinical data downloaded from Broad GDAC Firehose (https://gdac.broadinstitute.org/). It filters the emerging candidate SL pairs by prioritizing those whose co- inactivation is associated with better prognosis in patients. A stratified Cox proportional hazard model was used to check this association, while controlling for various confounding factors including cancer types, genomic instability[64], sex, age, and race:

$$h_g(t) \sim h_{0g}(t)\exp(\beta_1 I(A, B) + \beta_2 \text{age} + \beta_3 \text{GII}) \quad (1)$$

where g is an indicator variable over all possible combinations of patients' stratifications based on patients' sex, age, and tumor type. $h_g(t)$ is the hazard function (defined as the risk of death of patients per unit time), and $h_{0g}(t)$ is the baseline-hazard function at time t of the g^{th} stratification. The model contains three covariates: (i) I(*A, B*): indicator variable denoting if both ASNS and its candidate SL partner are downregulated in the patient's tumor, (ii) age: age of the patient, (iii) GII: genomic instability index. GII measures the relative amplification or deletion of genes in a tumor based on the SCNA. Given s_i be the absolute of log ratio of SCNA of gene i in a sample relative to normal control, GII of the sample is given as in Bilal *et al.*[64]:

$$GII = 1 / N \sum_1^N I(s_i > 1) . \quad (2)$$

The βs are the regression coefficient parameters of the covariates, which quantify the effect of covariates on the survival. All covariates are normalized to N(0,1). The βs are determined by standard likelihood maximization of the model[65] using the R-package "Survival".

Polysome Profiling

Polysome profiling was performed as described previously[23]. A375 cells were seeded at 30% confluency in a 15-cm Petri dish and transfected with NT-siRNA, si-*ASNS*, si-MNK1 (#1), or si-*ASNS* + si-*MNK1* for 16 hr, using JetPrime transfection reagent (Polyplus) as per manufacturer's instruction. Post-transfection, cells were replenished with fresh media containing vehicle (DMSO) or 500 nM PLX-4032 (Selleckchem) for 48 hr treatment. Cells were harvested at 80% confluency, washed twice with ice cold PBS containing 100 μg/mL cycloheximide and then lysed in hypotonic lysis buffer (5 mM Tris HCl pH 7.5, 2.5 mM $MgCl_2$, 1.5 mM KCl, 100 μg/ml cycloheximide, 2 mM dithiothreitol (DTT), 0.5% Triton, 0.5% sodium deoxycholate). Optical density values at 260 nm (OD_{260}) were measured in each lysate and OD_{260} of ~5 were then loaded in 5–50% sucrose gradients generated using Gradient Master (Biocomp, Fredericton, NB). 10% of lysates were saved as input samples for total RNA extraction. Sucrose gradients were subjected to ultracentrifugation (SW41 Ti 11E1698 rotor; Beckman 39,000 RPM for 2 hr at 4 °C) and fractionated by displacement using 60% sucrose/0.01% bromophenol blue, on ISCO Foxy fraction collector (35 sec for each fraction ~ 750 μL per fraction) equipped with an ultraviolet lamp for continuous absorbance monitoring at 254 nm. After fractionation, Trizol LS (Thermo-Fisher Scientific) was immediately added to all fractions and stored at −80 °C. Following RNA extraction from each fraction, RNA samples from subpolysomal fractions 6-8 (Pool 1), light fractions 9-11 (Pool 2), and heavy fractions 12-16 (Pool 3) were pooled. cDNA was synthesized using oligo(dT) and random primers (AB Bioscience), and qPCR analysis was performed with SYBR Green (Roche, NJ, USA). Relative change in the transcript levels in different pools was determined by the 2-ΔΔCT method, and shown as fold-change relative to mock-treated cells. β-Actin was used as an internal control.

In Vivo Studies

All experimental animal procedures were approved by the Institutional Animal Care and Use Committee (IACUC) of Sanford Burnham Prebys Medical Discovery Institute. IACUC

approval # for these studies were 18-001 (pancreatic cancer) and 18-079 (melaoma). Animal studies were conducted at Sanford Burnham Prebys Medical Discovery Institute Animal Facility in accordance with the IACUC guidelines. The study is compliant with all relevant ethical regulations regarding animal research. 8-week-old males C57BL/6 mice were purchased from Jackson laboratories (Bar Harbor, ME) and allowed to acclimatize for 1 week. $KRAS^{LSLG12D/+}$; $p53^{R172H/+;}$ $PDX^{Cretg/+}$ (KPC/B6) pancreatic cancer cells (1×10^6, suspended in 30 μl sterile PBS) were orthotopically injected into head of the pancreas. After one week, mice were randomized and sorted into treatment groups (n=8 animal/group). L-A'ase (60 IU/animal) was administered daily for five times a week for 3 weeks intraperitoneally. MEK inhibitor PD-325901 (4mg/kg) in 0.5% (w/v) hydroxy-propyl-methylcellulose, 0.2% (v/v) Tween 80 (Sigma) was administered by oral gavage twice a week for 3 weeks. For *in vivo* melanoma study, 8-week-old male C57BL/6 mice were injected subcutaneously in the flank with 2×10^5 MaNRAS1 (1007) cells. When tumors reached ~250 mm^3, mice were randomized and sorted into treatment groups (n=8 animal/group). L-A'ase and PD-3259011 were administered as above for the pancreatic tumor study for the duration indicated in Fig. 7h. For *in vivo* metastasis study, 6-week-old male C3H/HeN mice were injected subcutaneously with 2×10^5 SW1 melanoma cells. When tumors were palpable, mice were randomized (n=8 animal/group). L-A'ase and PD-3259011 (at 2.5 mg/Kg or 5.0 mg/Kg) were administered as noted for the pancreatic tumor study. Mice were sacrificed 28 days after therapy initiation. Metastasis was quantified by counting the number of tumor lesions on the anterior, posterior, diaphragmatic, and mediastinal surfaces of the lungs.

Mice were maintained in a pathogen-free environment with free access to food. Tumor volume was measured blinded twice a week. Tumor volume was measured with linear calipers and calculated using the formula: ([length in millimeters × (width in millimeters)^2]/2). After the mice were sacrificed, tumors were frozen or fixed in Z-Fix (Anatech, Battle Creek, MI) and embedded in paraffin for immunohistochemistry. Snap frozen tumors were utilized for protein and RNA extraction for further analysis.

Immunohistochemistry

5 mm sections were cut in a Leica Microsystems cryostat and transferred onto Superfrost-Plus slides (Thermo-Fisher Scientific), followed by staining with hematoxylin and eosin (H&E). For immunohistochemistry, the sections were deparaffinized and rehydrated, and antigen was retrieved using Dako target retrieval solution (Dako, Santa Clara, CA). To quench endogenous peroxidase activity incubation with 3% hydrogen peroxide for 30 min was performed. Specimens were incubated with cleaved caspase-3 antibody (Cell Signaling Technology), diluted in Dako antibody diluent overnight at 4 °C, followed by 3 washes with PBS/0.03% Tween-20 and incubation with Dako Labeled Polymer-HRP for 1 hr at room temperature. Following three washes with PBS containing 0.03% Tween-20, the sections were incubated with DAB chromogen and counterstained with hematoxylin.

Statistics and Reproducibility

Statistical significance between two groups was assessed by the unpaired Student's t-test. Ordinary one-way ANOVA was used to analyze more than two groups. Two-way ANOVA

was utilized to analyze cell proliferation at multiple timepoints. GraphPad Prism 7 and 8 software (Graphpad, La Jolla, CA) was used for to perform all statistical calculations. All cell culture experiments were performed three times, except 3f, which was performed two times. Data is presented as mean ± SEM (as noted in the figure legends) and a *P* value less than 0.05 was considered statistically significant.

Data Availability

The 28-cancer-type data were derived from the TCGA Research Network: http://cancergenome.nih.gov/. The data-set derived from this resource that supports the findings of this study is available in Broad GDAC Firehose (https://gdac.broadinstitute.org/). All patient's data was analyzed from published papers that are referenced and publicly available accordingly. Raw data for the GC-MS figures were deposited in Figshare with the Digital Object Identifier 10.6084/m9.figshare.9887984. All data supporting the findings of this study are available from the corresponding author on reasonable request.

Extended Data

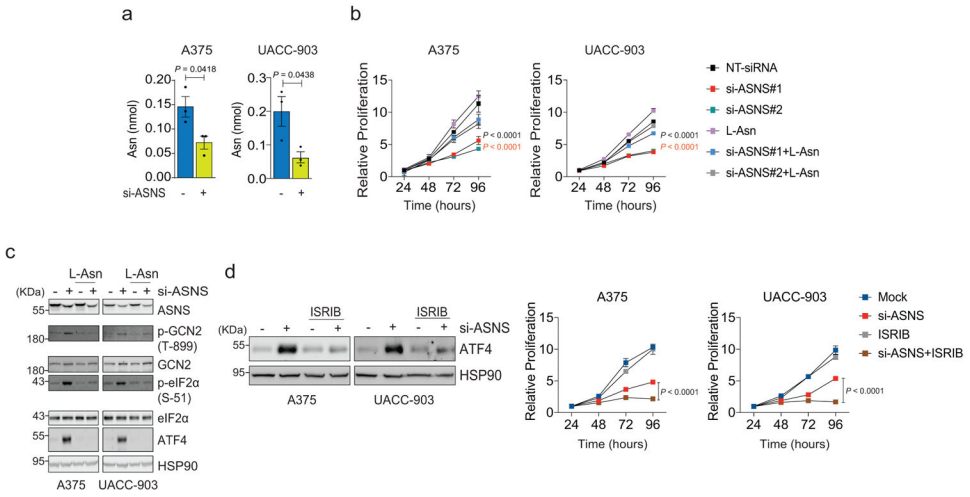

Extended Data Fig. 1. ASNS Suppression Induces the Amino Acid Response Pathway

a, GC-MS-based estimation of intracellular asparagine levels in A375 and UACC-903 cells 72 hr after treatment with si-*ASNS*. **b**, Relative proliferation of A375 and UACC-903 cells treated with si-*ASNS*#1 or si-*ASNS*#2, with or without supplementation with L-asparagine (L-Asn; 0.3 mM), over the indicated time course. **c**, Immunoblotting of ASNS, ATF4, phosphorylated and total GCN2 and eIF2α in melanoma cells 72 hr after treatment with si-*ASNS*, L-Asn (0.3 mM), or both. **d**, Immunoblotting of ATF4 in melanoma lines 72 hr after treatment with si-*ASNS*, ISRIB (200 nM), or both (left). Relative proliferation of melanoma cells treated as in (left) for indicated time course (right). Data are representative of three independent experiments and presented as mean ±SEM of n=3 biological replicates in **b** and **d**. Data shown as mean ±SEM of n=3 independent experiments in **a**. Statistical significance was calculated using two-tailed unpaired Student's t-test for **a** and two-way Anova for **b** and **d**. In **b**, black and orange P-values correspond to the comparison between si-*ASNS*#1 and si-*ASNS*#1+L-Asn and si-*ASNS*#2 and si-*ASNS*#2+L-Asn respectively.

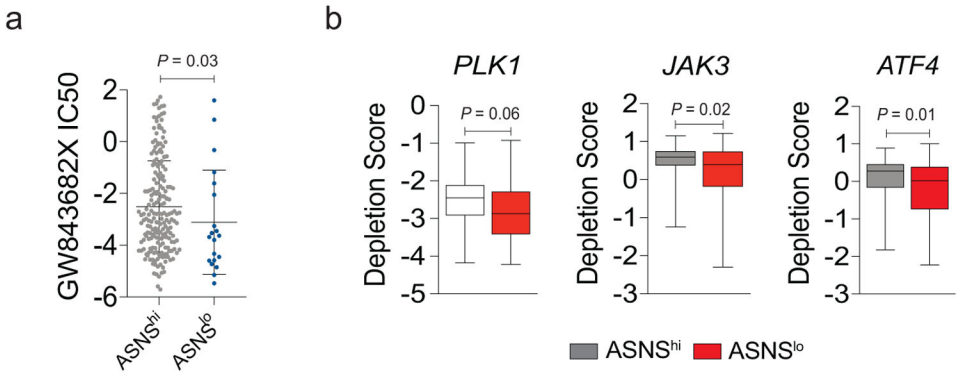

Extended Data Fig. 2. In-Silico Pan-Tumor Analysis Predicts Synthetic Lethal Partners of ASNS

a, Sensitivity to the PLK1/3 inhibitor GW843682X of pan-tumor cell lines segregated based on high (*ASNS*^{hi}) and low (*ASNS*^{lo}) *ASNS* expression. *P*-value calculated by one-sided Wilcoxon rank sum test. Each dot represents a cell line (*ASNS*^{hi}, n=204; *ASNS*^{lo}, n=20). Middle line and the whiskers represent the mean and the standard deviation respectively. **b**, Conditional essentiality of PLK1 (*ASNS*^{hi}, n=24; *ASNS*^{lo}, n=22), JAK3 (*ASNS*^{hi}, n=69; *ASNS*^{lo}, n=67) and ATF4 (*ASNS*^{hi}, n=69; *ASNS*^{lo}, n=67) in *ASNS*^{lo} and *ASNS*^{hi} cell lines. One-sided Wilcoxon rank sum *P*-values are denoted for each gene knockdown. GW843682X, PLK1 inhibitor. Data information: In the boxplots, the top and bottom horizontal lines represent the 75th and the 25th percentile, respectively, and the middle horizontal line represents the median. The size of the box represents the interquartile range, and the top and bottom whiskers represent the maximum and the minimum values respectively.

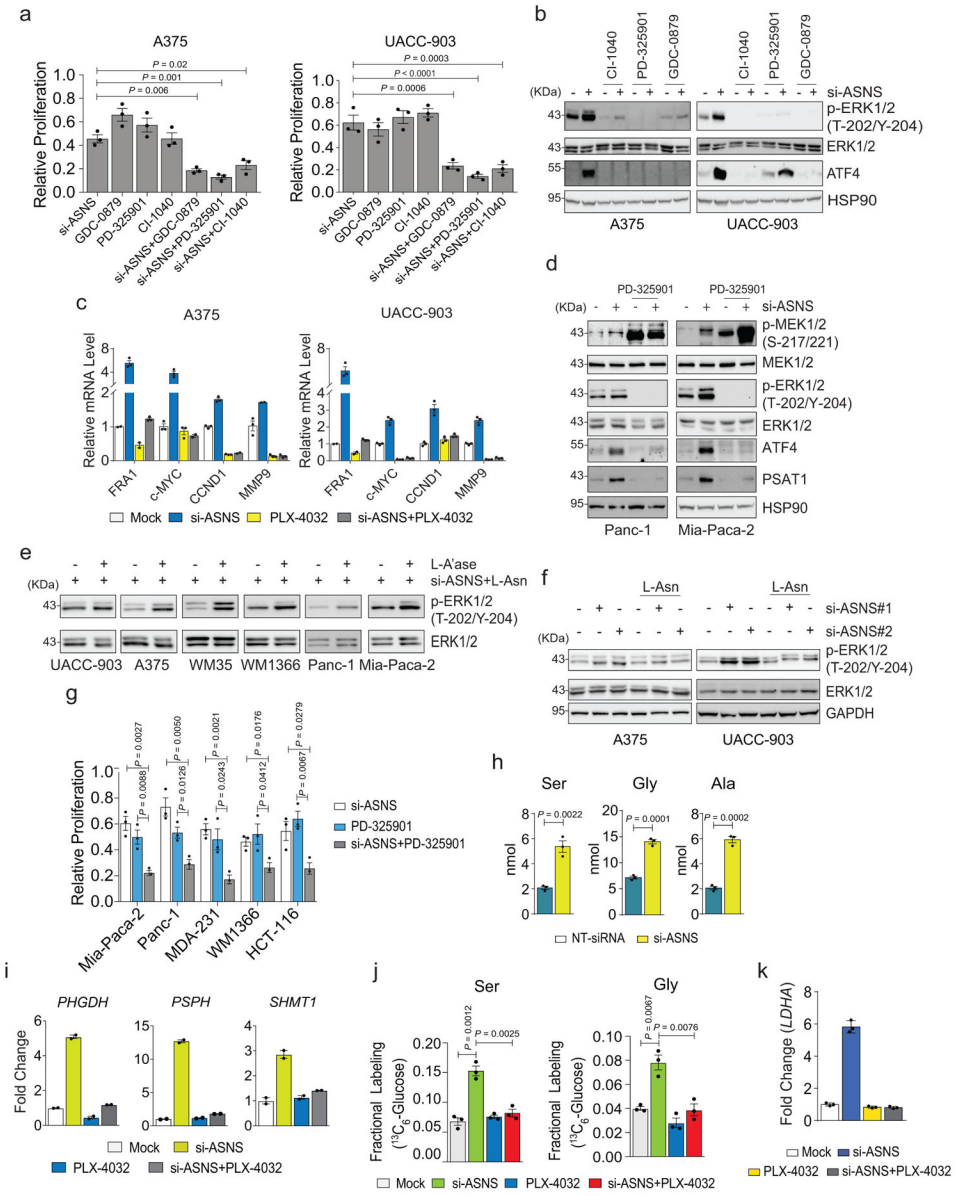

Extended Data Fig. 3. MAPK Signaling is Critical for ATF4 Induction Upon Asparagine Limitation

a, Proliferation of melanoma cells as measured 72 hr after indicated treatment. Proliferation is shown relative to mock (NT-siRNA and DMSO)-treated cells, set to 1.0. **b**, Immunoblotting of indicated proteins in melanoma cells 72 hr after indicated treatment. **c**, qRT-PCR analysis of indicated transcripts in melanoma cells 48 hr after treatment with si-*ASNS*, PLX-4032, or both. **d**, Immunoblotting of indicated proteins 72 hr after treatment with si-*ASNS*, PD-325901 or both. **e**, Immunoblotting of phosphorylated and total ERK1/2 protein in indicated cancer cell lines 72 hr after combined treatment with si-*ASNS* and L-Asn, with or without L-A'ase. **f**, Immunoblotting of phosphorylated ERK1/2 in melanoma cells 72 hr after treatment with si-*ASNS*#1 or #2, with or without supplementation with L-Asn. **g**, Proliferation of cancer cell lines measured 72 hr after treatment with si-*ASNS*,

PD-325901, or both relative to mock. **h**, GC-MS-based estimation of intracellular Ser, Gly, and Ala levels in UACC-903 cells 72 hr after treatment with si-*ASNS*. **i**, qRT-PCR analysis of indicated transcripts in UACC-903 cells 48 hr after treatment with si-*ASNS*, PLX-4032, or both. **j**, GC-MS-based $^{13}C_6$-glucose fractional isotope labeling of serine and glycine in UACC-903 cells 72 hr after treatment with si-*ASNS*, PLX-4032, or both. **k**, qRT-PCR analysis of *LDHA* transcript in UACC-903 cells 48 hr after indicated treatment. Data are representative of three independent experiments and presented as the mean ±SEM of n=3 biological replicates in **a** and **g**, mean ±SEM of n=3 technical replicates in **c** and **k**, mean ±SEM of n=2 technical replicates in **i**. Data shown as mean ±SEM of n=3 independent experiments in **h** and **j**. Statistical significance was calculated using two-tailed unpaired Student's *t*-test, except in **a**, where ordinary one-way Anova was used.

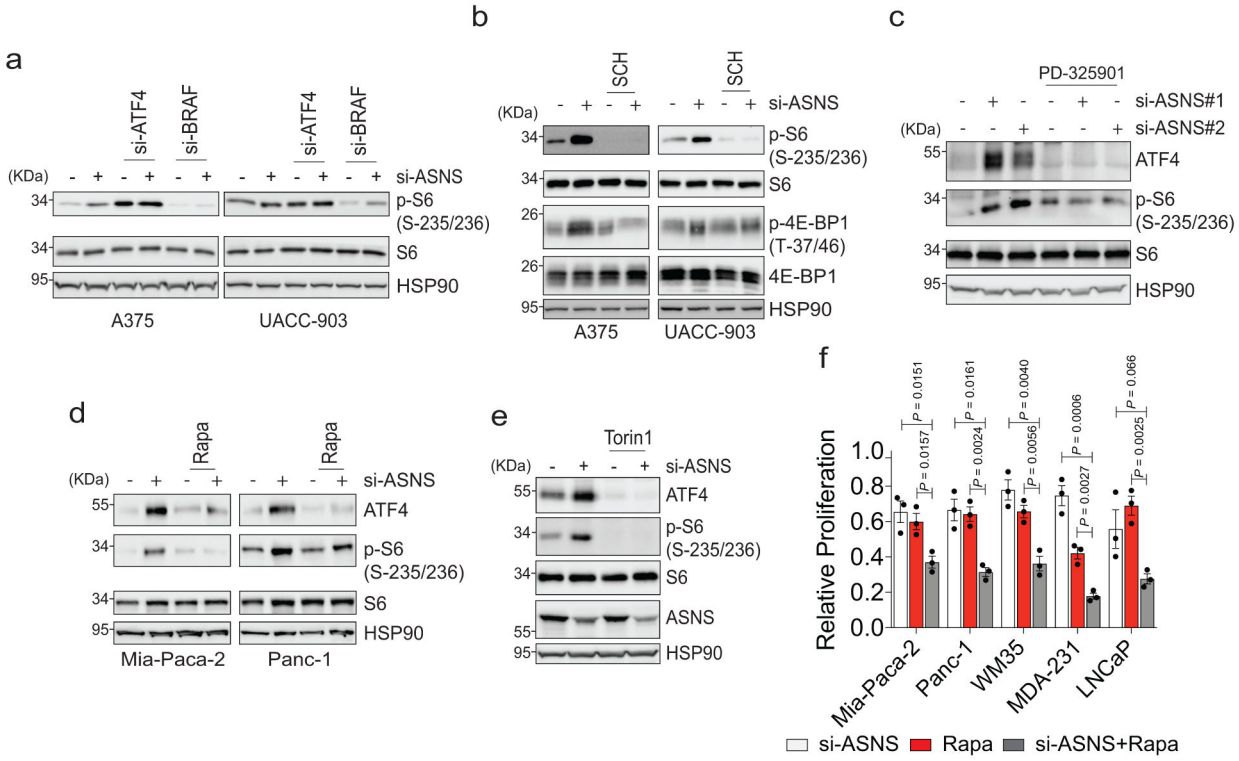

Extended Data Fig. 4. The MAPK-mTORC1-eIF4E Axis is Essential for ATF4 Induction Following Asparagine Limitation

a, Immunoblotting of phosphorylated and total S6 protein in melanoma cells 72 hr after treatment with si-*ASNS*, si-*ATF4*, si-*BRAF*, or indicated combinations. Fig. 3d and Extended Data Fig. 4a show parts of the same experiment and share the internal control (HSP90). **b**, Immunoblotting of phosphorylated and total S6 protein and 4E-BP1 in melanoma cells 72 hr after treatment with si-*ASNS*, SCH-772984, or both. **c**, Immunoblotting of ATF4 and phosphorylated and total S6 protein in Mia-Paca-2 cells 72 hr after treatment with si-*ASNS*#1 or #2, PD-325901, or a combination of the respective si-*ASNS* and PD-325901. **d**, Immunoblotting of ATF4 and phosphorylated and total S6 protein in pancreatic cancer cell lines 72 hr after treatment with si-*ASNS*, Rapamycin (Rapa), or both. **e**, Immunoblotting of ATF4 and phosphorylated and total S6 protein in Mia-Paca-2 cells 72 hr after treatment with si-*ASNS*, Torin 1, or both. **f**, Proliferation of cancer cell lines measured 72 hr after treatment with si-*ASNS*, Rapa, or both. Values are shown relative to mock (NT-siRNA and DMSO)-treated cells. Data are representative of three independent experiments and presented as the mean ±SEM of n=3 biological replicates in **f**. Statistical significance was calculated using two-tailed unpaired Student's t-test.

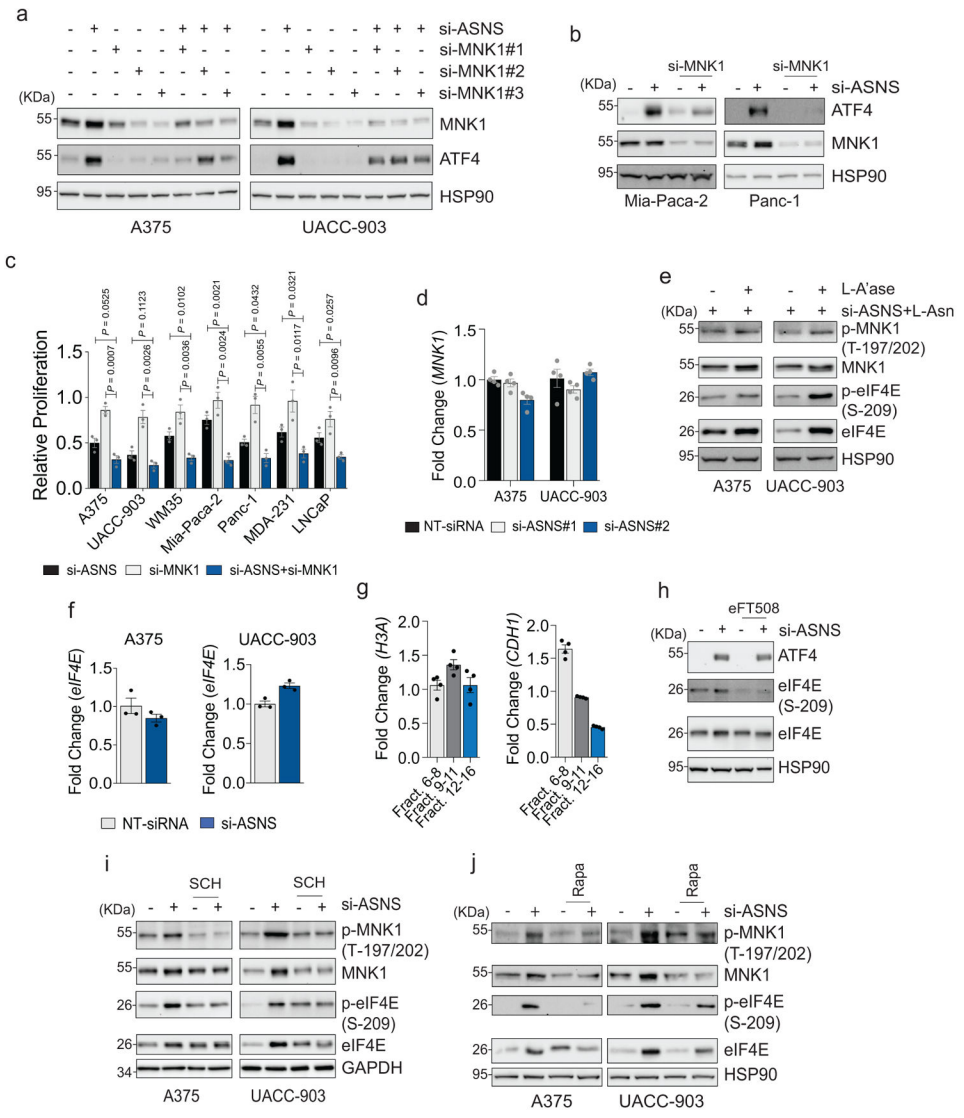

Extended Data Fig. 5. MNK1 is Critical for ASNS Suppression-Associated ATF4 Induction

a, Immunoblotting of MNK1 and ATF4 in melanoma cells 72 hr after treatment with si-*ASNS*, si-*MNK1*#1, #2 or #3, or indicated combinations of si-*ASNS* with si-*MNK1*#1-#3. **b**, Immunoblotting of ATF4 and MNK1 in Mia-Paca-2 and Panc-1 cells 72 hr after treatment with si-*ASNS*, si-*MNK1*, or both. **c**, Proliferation of cancer cell lines 72 hr after treatment with si-*ASNS*, si-*MNK1*, or both relative to NT-siRNA treated cells (set to 1.0). **d**, qRT-PCR analysis of *MNK1* transcript in melanoma cells 48 hr after treatment with indicated si-*ASNS*. **e**, Immunoblotting of phospho and total MNK1 and eIF4E proteins in melanoma cells after 72 hr treatment with si-*ASNS* and L-Asn (0.3 mM), with or without L-A'ase. **f**, qRT-PCR analysis of *eIF4E* transcript in melanoma cells 48 hr after treatment with si-*ASNS*. **g**, qRT-PCR analysis of *H3A* and *CDH1* mRNA levels in subpolysomal, light, and heavy polysomal fractions of A375 cells treated for 48 hr with si-*ASNS* relative to mock treatment, set to 1.0. **h**, Immunoblotting of ATF4 and phospho and total eIF4E protein in UACC-903 cells treated with si-*ASNS*, eFT508, or both for 72 hr. **i** and **j**, Immunoblotting of phospho

and total MNK1 and eIF4E proteins in melanoma cells treated 72 hr with si-*ASNS*, SCH-772984, or both (**i**), or si-*ASNS*, Rapa, or both (**j**). Data are representative of three independent experiments and presented as the mean ±SEM of n=3 biological replicates in **c**, mean ±SEM of n=4 technical replicates in **d** and **g**, and mean ±SEM of n=3 technical replicates in **f**. Statistical significance was calculated using two-tailed unpaired Student's *t*-test.

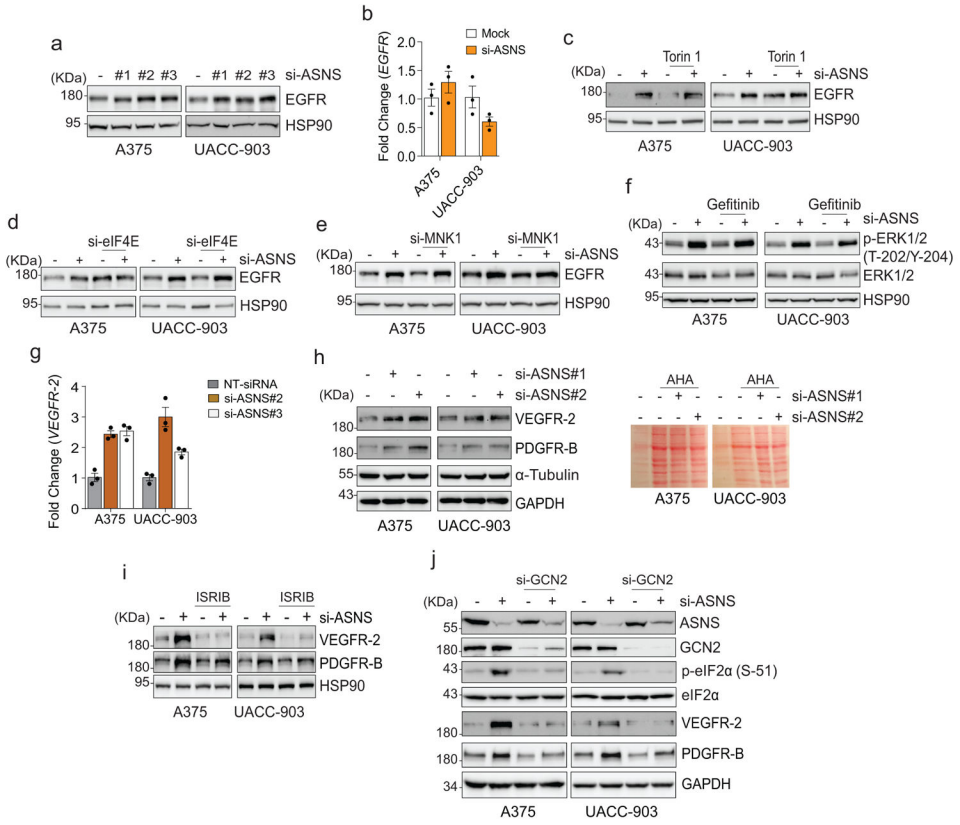

Extended Data Fig. 6. Asparagine Limitation Increases RTK Expression

a, Immunoblotting of EGFR in melanoma cells 72 hr after treatment with indicated si-*ASNS*. **b**, qRT-PCR analysis of *EGFR* transcript in melanoma cells 48 hr after treatment with si-*ASNS*. **c-e**, Immunoblotting of EGFR in melanoma cells 72 hr after treatment either individually or as a combination with si-*ASNS* and Torin 1 (**c**), si-*ASNS* and si-*eIF4E* (**d**), or si-*ASNS* and si-*MNK1* (**e**). **f**, Immunoblotting of phospho and total ERK1/2 in melanoma cells treated 72 hr with si-*ASNS*, EGFR inhibitor (Gefitinib), or both. **g**, qRT-PCR analysis of *VEGFR-2* transcript levels in melanoma cells 48 hr after treatment with si-*ASNS*#2 or #3. **h**, (left) Immunoblotting of VEGFR-2, PDGFR-B, α-Tubulin, and GAPDH in melanoma cells treated with NT-siRNA, si-*ASNS*#1 or #2 followed by L-azidohomoalanine (AHA) labeling (see Methods). (right) Ponseau-S staining of streptavidin pull-down fraction from melanoma cells left untreated or treated with AHA. **i**, Immunoblotting of VEGFR-2 and PDGFR-B in melanoma cells 72 hr after treatment with si-*ASNS*, ISRIB, or both. **j**, Immunoblotting of the indicated proteins in melanoma cells 72 hr after treatment with si-*ASNS*, si-*GCN2*, or both. Data are representative of three independent experiments and presented as the mean ±SEM of n=3 technical replicates in **b** and **g**.

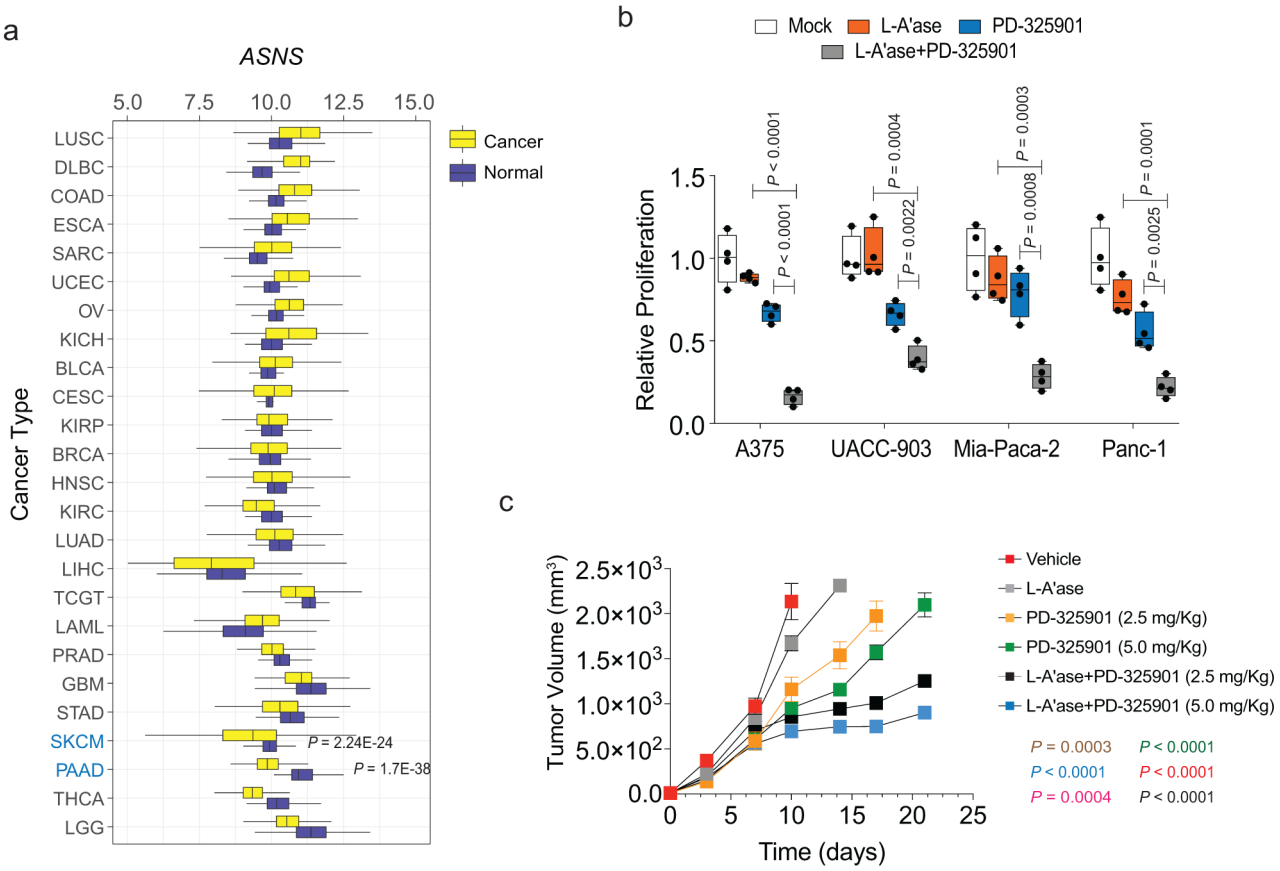

Extended Data Fig. 7. L-Asparaginase and MEK Inhibitor Combination Suppresses In Vivo Tumor Growth

a, Comparison of ASNS expression in cancer vs. healthy tissue samples from TCGA dataset using two-sided Wilcoxon rank sum test. **b**, Proliferation of melanoma and pancreatic cancer cell lines as measured 72 hr after treatment with L-A'ase, PD-325901, or both relative to mock-treated cells. All cell lines were grown in L-Asn-supplemented DMEM. **c**, Volume of tumors from C3H/HeN mice injected subcutaneously with SW1 mouse melanoma cells and treated as indicated (n=8 mice per group). Statistical analysis: Welch's t-test (two-tailed). In **c**, brown, blue, and pink P-values correspond to the comparison between L-A'ase +PD-325901 (2.5 mg/Kg) and Vehicle, L-A'ase+PD-325901 (2.5 mg/Kg) and L-A'ase, and L-A'ase+PD-325901(2.5 mg/Kg) and PD-325901 (2.5 mg/Kg) respectively. In c, green, red, and black P-values correspond to the comparison between L-A'ase+PD-325901(5.0 mg/Kg) and Vehicle, L-A'ase+PD-325901 (5.0 mg/Kg) and L-A'ase, and L-A'ase+PD-325901(5.0 mg/Kg) and PD-325901 (5.0 mg/Kg) respectively. In **a**, LUSC, Lung Squamous Cell Carcinoma; DLBC, Diffuse Large B-Cell Lymphoma; COAD, Colon Adenocarcinoma; ESCA, Esophageal Carcinoma; SARC, Sarcoma; UCEC, Uterine Corpus Endometrial Carcinoma; OV, Ovarian Cancer; KICH, Kidney Chromophobe; BLCA, Bladder Urothelial Carcinoma; CESC, Cervical Squamous Cell Carcinoma; KIRP, Kidney Renal Papillary Cell Carcinoma; BRCA, Breast Cancer; HNSC, Head and Neck Squamous Cell Carcinoma; KIRC, Kidney Renal Clear Cell Carcinoma; LUAD, Lung Adenocarcinoma; LIHC, Liver Hepatocellular Carcinoma; TCGT, Tenosynovial Giant Cell Tumor; LAML, Acute Myeloid

Leukemia; PRAD, Prostate Adenocarcinoma; GBM, Glioblastoma Multiforme; STAD, Stomach Adenocarcinoma; THCA, Thyroid Carcinoma; LGG, Low Grade Glioma. Data information: In the boxplots, the top and bottom horizontal lines represent the 75th and the 25th percentile, respectively, and the middle horizontal line represents the median. The size of the box represents the interquartile range, and the top and bottom whiskers represent the maximum and the minimum values respectively. In **b**, data are representative of three independent experiments and presented as the mean ±SEM of n=4 biological replicates and the statistical significance was calculated using two-tailed unpaired Student's t-test.

Supplementary Material

Refer to Web version on PubMed Central for supplementary material.

Acknowledgements

We thank David Tuveson and lab members for providing KPC cells, Meenhard Herlyn for providing the melanoma cell lines, members of the Lionel Larue lab for establishing the NRAS mutant melanoma cell line MaNRAS1 (1007), Matthew Leibovitch for technical assistance, Olga Zagnitko for metabolic analyses, and members of the Ronai lab for continued discussion. The Cancer Metabolism Core at Sanford Burnham Prebys Medical Discovery Institute is supported by NCI Cancer Center Support Grant P30CA030199. IT is a scholar of the Fonds de Recherche du Québec-Santé (FRQS; Junior 2). Support from NCI grants R35CA197465, P01CA128814 and Hevery Foundation Gift (to ZR) are gratefully acknowledged.

References

1. Maddocks ODK et al. Modulating the therapeutic response of tumours to dietary serine and glycine starvation. Nature 544, 372–376, doi:10.1038/nature22056 (2017). [PubMed: 28425994]
2. Sun L et al. cMyc-mediated activation of serine biosynthesis pathway is critical for cancer progression under nutrient deprivation conditions. Cell Res 25, 429–444, doi:10.1038/cr.2015.33 (2015). [PubMed: 25793315]
3. Wise DR & Thompson CB Glutamine addiction: a new therapeutic target in cancer. Trends Biochem Sci 35, 427–433, doi:10.1016/j.tibs.2010.05.003 (2010). [PubMed: 20570523]
4. Altman BJ, Stine ZE & Dang CV From Krebs to clinic: glutamine metabolism to cancer therapy. Nat Rev Cancer 16, 749, doi:10.1038/nrc.2016.114 (2016). [PubMed: 28704361]
5. Pavlova NN et al. As Extracellular Glutamine Levels Decline, Asparagine Becomes an Essential Amino Acid. Cell Metab 27, 428–438 e425, doi:10.1016/j.cmet.2017.12.006 (2018). [PubMed: 29337136]
6. Zhang J et al. Asparagine plays a critical role in regulating cellular adaptation to glutamine depletion. Mol Cell 56, 205–218, doi:10.1016/j.molcel.2014.08.018 (2014). [PubMed: 25242145]
7. Knott SRV et al. Asparagine bioavailability governs metastasis in a model of breast cancer. Nature 554, 378–381, doi:10.1038/nature25465 (2018). [PubMed: 29414946]
8. Gwinn DM et al. Oncogenic KRAS Regulates Amino Acid Homeostasis and Asparagine Biosynthesis via ATF4 and Alters Sensitivity to L-Asparaginase. Cancer Cell 33, 91–107 e106, doi:10.1016/j.ccell.2017.12.003 (2018). [PubMed: 29316436]
9. Pieters R et al. L-asparaginase treatment in acute lymphoblastic leukemia: a focus on Erwinia asparaginase. Cancer 117, 238–249, doi:10.1002/cncr.25489 (2011). [PubMed: 20824725]
10. Stams WA et al. Asparagine synthetase expression is linked with L-asparaginase resistance in TEL-AML1-negative but not TEL-AML1-positive pediatric acute lymphoblastic leukemia. Blood 105, 4223–4225, doi:10.1182/blood-2004-10-3892 (2005). [PubMed: 15718422]
11. Lessner HE, Valenstein S, Kaplan R, DeSimone P & Yunis A Phase II study of L-asparaginase in the treatment of pancreatic carcinoma. Cancer Treat Rep 64, 1359–1361 (1980). [PubMed: 7471124]

12. Bachet JB et al. Asparagine Synthetase Expression and Phase I Study With L-Asparaginase Encapsulated in Red Blood Cells in Patients With Pancreatic Adenocarcinoma. Pancreas 44, 1141–1147, doi:10.1097/MPA.0000000000000394 (2015). [PubMed: 26355551]
13. Taylor CW, Dorr RT, Fanta P, Hersh EM & Salmon SE A phase I and pharmacodynamic evaluation of polyethylene glycol-conjugated L-asparaginase in patients with advanced solid tumors. Cancer Chemother Pharmacol 47, 83–88, doi:10.1007/s002800000207 (2001). [PubMed: 11221967]
14. Kilberg MS, Shan J & Su N ATF4-dependent transcription mediates signaling of amino acid limitation. Trends Endocrinol Metab 20, 436–443, doi:10.1016/j.tem.2009.05.008 (2009). [PubMed: 19800252]
15. Nakamura A et al. Inhibition of GCN2 sensitizes ASNS-low cancer cells to asparaginase by disrupting the amino acid response. Proc Natl Acad Sci U S A 115, E7776–E7785, doi:10.1073/pnas.1805523115 (2018). [PubMed: 30061420]
16. Lee JS et al. Harnessing synthetic lethality to predict the response to cancer treatment. Nat Commun 9, 2546, doi:10.1038/s41467-018-04647-1 (2018). [PubMed: 29959327]
17. Bramham CR, Jensen KB & Proud CG Tuning Specific Translation in Cancer Metastasis and Synaptic Memory: Control at the MNK-eIF4E Axis. Trends Biochem Sci 41, 847–858, doi:10.1016/j.tibs.2016.07.008 (2016). [PubMed: 27527252]
18. Wu J, Ivanov AI, Fisher PB & Fu Z Polo-like kinase 1 induces epithelial-to-mesenchymal transition and promotes epithelial cell motility by activating CRAF/ERK signaling. Elife 5, doi:10.7554/eLife.10734 (2016).
19. Eferl R & Wagner EF AP-1: a double-edged sword in tumorigenesis. Nat Rev Cancer 3, 859–868, doi:10.1038/nrc1209 (2003). [PubMed: 14668816]
20. Sears R et al. Multiple Ras-dependent phosphorylation pathways regulate Myc protein stability. Genes Dev 14, 2501–2514 (2000). [PubMed: 11018017]
21. Balgi AD et al. Regulation of mTORC1 signaling by pH. PLoS One 6, e21549, doi:10.1371/journal.pone.0021549 (2011). [PubMed: 21738705]
22. Roux PP & Topisirovic I Signaling Pathways Involved in the Regulation of mRNA Translation. Mol Cell Biol 38, doi:10.1128/MCB.00070-18 (2018).
23. Gandin V et al. Polysome fractionation and analysis of mammalian translatomes on a genome-wide scale. J Vis Exp, doi:10.3791/51455 (2014).
24. Waskiewicz AJ et al. Phosphorylation of the cap-binding protein eukaryotic translation initiation factor 4E by protein kinase Mnk1 in vivo. Mol Cell Biol 19, 1871–1880, doi:10.1128/mcb.19.3.1871 (1999). [PubMed: 10022874]
25. Wendel HG et al. Dissecting eIF4E action in tumorigenesis. Genes Dev 21, 3232–3237, doi:10.1101/gad.1604407 (2007). [PubMed: 18055695]
26. Topisirovic I, Ruiz-Gutierrez M & Borden KL Phosphorylation of the eukaryotic translation initiation factor eIF4E contributes to its transformation and mRNA transport activities. Cancer Res 64, 8639–8642,oi:10.1158/0008-5472.CAN-04-2677 (2004). [PubMed: 15574771]
27. Waskiewicz AJ, Flynn A, Proud CG & Cooper JA Mitogen-activated protein kinases activate the serine/threonine kinases Mnk1 and Mnk2. EMBO J 16, 1909–1920, doi:10.1093/emboj/16.8.1909 (1997). [PubMed: 9155017]
28. Furic L et al. eIF4E phosphorylation promotes tumorigenesis and is associated with prostate cancer progression. Proc Natl Acad Sci U S A 107, 14134–14139, doi:10.1073/pnas.1005320107 (2010). [PubMed: 20679199]
29. Webb TE, Hughes A, Smalley DS & Spriggs KA An internal ribosome entry site in the 5' untranslated region of epidermal growth factor receptor allows hypoxic expression. Oncogenesis 4, e134, doi:10.1038/oncsis.2014.43 (2015). [PubMed: 25622307]
30. Guan BJ et al. A Unique ISR Program Determines Cellular Responses to Chronic Stress. Mol Cell 68, 885–900 e886, doi:10.1016/j.molcel.2017.11.007 (2017). [PubMed: 29220654]
31. de la Parra C et al. A widespread alternate form of cap-dependent mRNA translation initiation. Nat Commun 9, 3068, doi:10.1038/s41467-018-05539-0 (2018). [PubMed: 30076308]
32. Liu S et al. METTL13 Methylation of eEF1A Increases Translational Output to Promote Tumorigenesis. Cell 176, 491–504 e421, doi:10.1016/j.cell.2018.11.038 (2019). [PubMed: 30612740]

33. Dorard C et al. RAF proteins exert both specific and compensatory functions during tumour progression of NRAS-driven melanoma. Nat Commun 8, 15262, doi:10.1038/ncomms15262 (2017). [PubMed: 28497782]
34. Bhoumik A et al. An ATF2-derived peptide sensitizes melanomas to apoptosis and inhibits their growth and metastasis. J Clin Invest 110, 643–650, doi:10.1172/JCI16081 (2002). [PubMed: 12208865]
35. Falletta P et al. Translation reprogramming is an evolutionarily conserved driver of phenotypic plasticity and therapeutic resistance in melanoma. Genes Dev 31, 18–33, doi:10.1101/gad.290940.116 (2017). [PubMed: 28096186]
36. Kakavand H et al. PD-L1 Expression and Immune Escape in Melanoma Resistance to MAPK Inhibitors. Clin Cancer Res 23, 6054–6061, doi:10.1158/1078-0432.CCR-16-1688 (2017). [PubMed: 28724663]
37. Rizos H et al. BRAF inhibitor resistance mechanisms in metastatic melanoma: spectrum and clinical impact. Clin Cancer Res 20, 1965–1977, doi:10.1158/1078-0432.CCR-13-3122 (2014). [PubMed: 24463458]
38. Kwong LN et al. Co-clinical assessment identifies patterns of BRAF inhibitor resistance in melanoma. J Clin Invest 125, 1459–1470, doi:10.1172/JCI78954 (2015). [PubMed: 25705882]
39. Zhang G et al. Targeting mitochondrial biogenesis to overcome drug resistance to MAPK inhibitors. J Clin Invest 126, 1834–1856, doi:10.1172/JCI82661 (2016). [PubMed: 27043285]
40. Wek RC Role of eIF2alpha Kinases in Translational Control and Adaptation to Cellular Stress. Cold Spring Harb Perspect Biol 10, doi:10.1101/cshperspect.a032870 (2018).
41. Krall AS, Xu S, Graeber TG, Braas D & Christofk HR Asparagine promotes cancer cell proliferation through use as an amino acid exchange factor. Nat Commun 7, 11457, doi:10.1038/ncomms11457 (2016). [PubMed: 27126896]
42. Pathria G et al. Targeting the Warburg effect via LDHA inhibition engages ATF4 signaling for cancer cell survival. EMBO J 37, doi:10.15252/embj.201899735 (2018).
43. Young SK & Wek RC Upstream Open Reading Frames Differentially Regulate Gene-specific Translation in the Integrated Stress Response. J Biol Chem 291, 16927–16935, doi:10.1074/jbc.R116.733899 (2016). [PubMed: 27358398]
44. Chen R et al. The general amino acid control pathway regulates mTOR and autophagy during serum/glutamine starvation. J Cell Biol 206, 173–182, doi:10.1083/jcb.201403009 (2014). [PubMed: 25049270]
45. Shin S et al. ERK2 Mediates Metabolic Stress Response to Regulate Cell Fate. Mol Cell 59, 382–398, doi:10.1016/j.molcel.2015.06.020 (2015). [PubMed: 26190261]
46. Thiaville MM et al. MEK signaling is required for phosphorylation of eIF2alpha following amino acid limitation of HepG2 human hepatoma cells. J Biol Chem 283, 10848–10857, doi:10.1074/jbc.M708320200 (2008). [PubMed: 18287093]
47. Oakes SA & Papa FR The role of endoplasmic reticulum stress in human pathology. Annu Rev Pathol 10, 173–194, doi:10.1146/annurev-pathol-012513-104649 (2015). [PubMed: 25387057]
48. Fiorese CJ et al. The Transcription Factor ATF5 Mediates a Mammalian Mitochondrial UPR. Curr Biol 26, 2037–2043, doi:10.1016/j.cub.2016.06.002 (2016). [PubMed: 27426517]
49. Pereira ER, Frudd K, Awad W & Hendershot LM Endoplasmic reticulum (ER) stress and hypoxia response pathways interact to potentiate hypoxia-inducible factor 1 (HIF-1) transcriptional activity on targets like vascular endothelial growth factor (VEGF). J Biol Chem 289, 3352–3364, doi:10.1074/jbc.M113.507194 (2014). [PubMed: 24347168]
50. Lu D, Wolfgang CD & Hai T Activating transcription factor 3, a stress-inducible gene, suppresses Ras-stimulated tumorigenesis. J Biol Chem 281, 10473–10481, doi:10.1074/jbc.M509278200 (2006). [PubMed: 16469745]
51. Sang N et al. MAPK signaling up-regulates the activity of hypoxia-inducible factors by its effects on p300. J Biol Chem 278, 14013–14019, doi:10.1074/jbc.M209702200 (2003). [PubMed: 12588875]
52. Wethmar K et al. Comprehensive translational control of tyrosine kinase expression by upstream open reading frames. Oncogene 35, 1736–1742, doi:10.1038/onc.2015.233 (2016). [PubMed: 26096937]

53. Calvo SE, Pagliarini DJ & Mootha VK Upstream open reading frames cause widespread reduction of protein expression and are polymorphic among humans. Proc Natl Acad Sci U S A 106, 7507–7512, doi:10.1073/pnas.0810916106 (2009). [PubMed: 19372376]
54. Ingolia NT, Lareau LF & Weissman JS Ribosome profiling of mouse embryonic stem cells reveals the complexity and dynamics of mammalian proteomes. Cell 147, 789–802, doi:10.1016/j.cell.2011.10.002 (2011). [PubMed: 22056041]
55. Sidrauski C, McGeachy AM, Ingolia NT & Walter P The small molecule ISRIB reverses the effects of eIF2alpha phosphorylation on translation and stress granule assembly. Elife 4, doi:10.7554/eLife.05033 (2015).
56. Reddy KB, Nabha SM & Atanaskova N Role of MAP kinase in tumor progression and invasion. Cancer Metastasis Rev 22, 395–403 (2003). [PubMed: 12884914]
57. Ackermann J et al. Metastasizing melanoma formation caused by expression of activated N-RasQ61K on an INK4a-deficient background. Cancer Res 65, 4005–4011, doi:10.1158/0008-5472.CAN-04-2970 (2005). [PubMed: 15899789]
58. Ratnikov B et al. Glutamate and asparagine cataplerosis underlie glutamine addiction in melanoma. Oncotarget 6, 7379–7389, doi:10.18632/oncotarget.3132 (2015). [PubMed: 25749035]
59. Marcotte R et al. Functional Genomic Landscape of Human Breast Cancer Drivers, Vulnerabilities, and Resistance. Cell 164, 293–309, doi:10.1016/j.cell.2015.11.062 (2016). [PubMed: 26771497]
60. Cowley GS et al. Parallel genome-scale loss of function screens in 216 cancer cell lines for the identification of context-specific genetic dependencies. Sci Data 1, 140035, doi:10.1038/sdata.2014.35 (2014). [PubMed: 25984343]
61. Marcotte R et al. Essential gene profiles in breast, pancreatic, and ovarian cancer cells. Cancer Discov 2, 172–189, doi:10.1158/2159-8290.CD-11-0224 (2012). [PubMed: 22585861]
62. Iorio F et al. A Landscape of Pharmacogenomic Interactions in Cancer. Cell 166, 740–754, doi:10.1016/j.cell.2016.06.017 (2016). [PubMed: 27397505]
63. Sahu AD et al. Genome-wide prediction of synthetic rescue mediators of resistance to targeted and immunotherapy. Mol Syst Biol 15, e8323, doi:10.15252/msb.20188323 (2019). [PubMed: 30858180]
64. Bilal E et al. Improving breast cancer survival analysis through competition-based multidimensional modeling. PLoS Comput Biol 9, e1003047, doi:10.1371/journal.pcbi.1003047 (2013). [PubMed: 23671412]
65. Therneau TM & Grambsch PM Modeling survival data : extending the Cox model. (Springer, 2000).

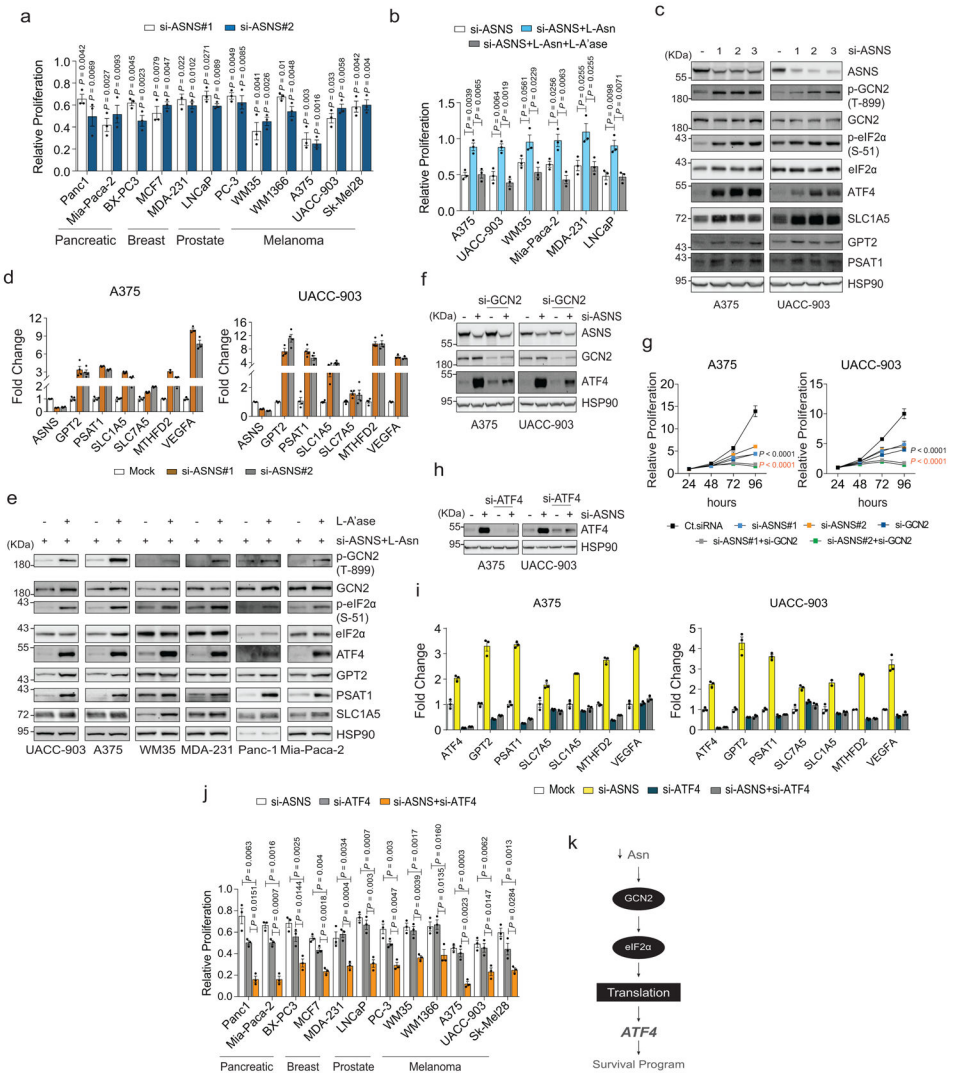

Fig. 1: ATF4 Activity Impedes Growth Suppression in Response to Asparagine Limitation.

a and **b**, Proliferation of indicated cancer cell lines 48 hr after transfection with si-*ASNS*#1 or si-*ASNS*#2 relative to non-targeting (NT)-siRNA transfected cells (value set to 1.0; **a**). Proliferation of cancer cell lines 72 hr after indicated treatment (**b**). L-asparagine (L-Asn; 0.3 mM) and L-Asparaginase (L-A'ase, 1U/ml). Data are shown relative to mock (NT-siRNA+d$H_2$0)-treated cells. **c**, Immunoblotting of amino acid response (AAR) pathway proteins in indicated cells 72 hr after treatment with si-*ASNS*#1, #2, or #3. **d**, qRT-PCR of transcripts encoding ATF4 targets in indicated cells 48 hr after treatment with si-*ASNS*#1 or #2. **e**, Immunoblotting of AAR pathway proteins in indicated cancer cell lines 72 hr after treatment with si-*ASNS* and L-Asn, with or without L-A'ase. **f**, Immunoblotting of ASNS, GCN2, and ATF4 in melanoma cells 72 hr after treatment with si-*ASNS*, si-*GCN2*, or both. **g**, Proliferation of melanoma cells over indicated times following treatment with si-*ASNS*, si-*GCN2*, or both. **h**, Immunoblotting of ATF4 in melanoma cells 72 hr after treatment with si-*ASNS*, si-*ATF4*, or both. **i**, qRT-PCR of transcripts encoding ATF4 targets in indicated cells treated as in **h** for 48 hr. **j**, Proliferation of cancer cell lines treated as in **h** for 48 hr. **k**,

Model depicting the pathway of ATF4 induction following ASNS suppression. Data are representative of three independent experiments and presented as the mean ± SEM of n=3 biological replicates in **a**, **b**, **g**, and **j** and mean ± SEM of n=4 and n=3 technical replicates in **d** and **i** respectively. Statistical significance was calculated using two-tailed unpaired Student's *t*-test except in **g**, where two-way Anova was used. In **g**, *P*-values in black and orange correspond to the comparison between si-*ASNS*#1 and si-*ASNS*#1+si-*GCN2* and si-*ASNS*#2 and si-*ASNS*#2+si-*GCN2* respectively.

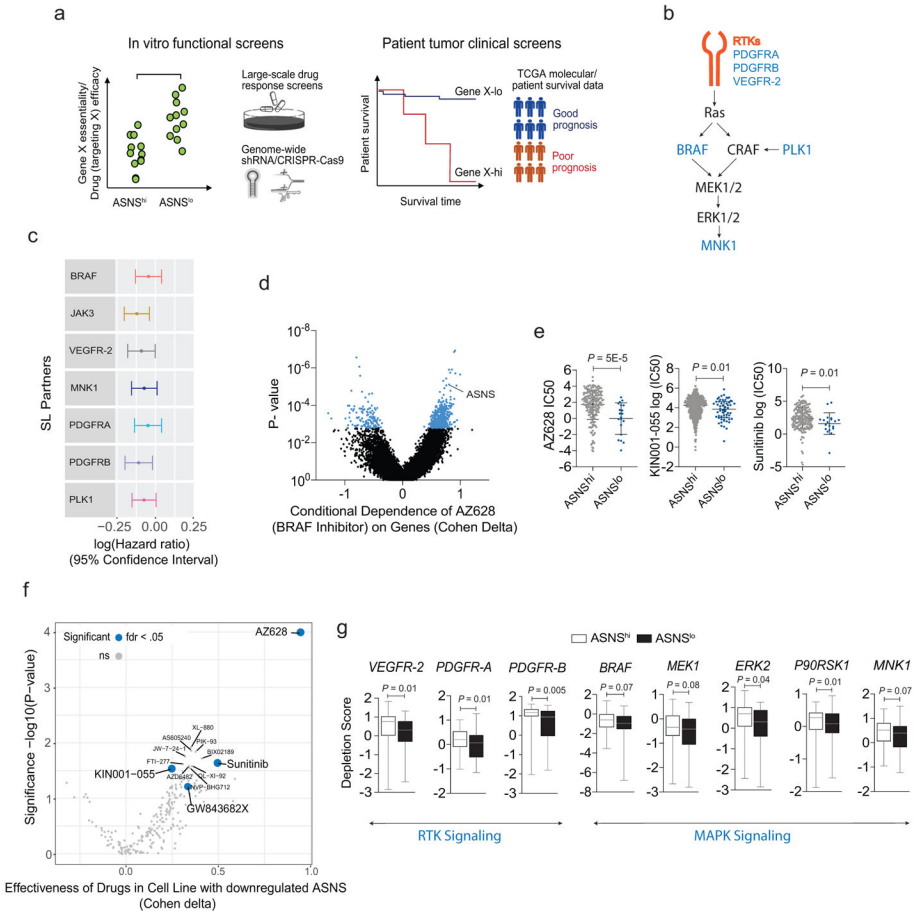

Fig. 2: In-Silico Pan-Tumor Analysis Predicts RTKs, BRAF, and MNK1 as ASNS Synthetic Lethal Partners.

a, Schematic showing the pipeline comprising functional *in vitro* and patient tumor clinical screens, to identify synthetic lethal partners of ASNS. **b**, Schematic representation of ASNS SL partners in the context of the MAPK signaling pathway. **c**, Forest plot depicting the reduction in cancer-related death risk when the identified SL partners are underexpressed together with *ASNS*. x-axis shows the hazard ratio in logarithmic scale, and y-axis shows the identified SL partners. The dots denote the hazard ratios, and error bars denote their confidence interval. The analysis was performed using 8,749 TCGA samples (see Methods). **d**, Volcano plot depicting sensitivity to BRAF inhibitor AZ628 as a function of gene expression of pan-genes. Significance was evaluated using two-sided Wilcoxon rank sum test comparing the sensitivity to AZ628 in cell lines with high (n=565) vs. low (n=63) expression of each gene. **e**, Sensitivity to the BRAF inhibitor AZ628, JAK3/MNK1 inhibitor KIN001-055, and pan-RTK inhibitor sunitinib of pan-cancer cell lines segregated based on high (*ASNS*^{hi}) and low (*ASNS*^{lo}) *ASNS* expression. Each dot represents a cell line, AZ628 (*ASNS*^{hi}, n=203; *ASNS*^{lo}, n=20); KIN001-055 (*ASNS*^{hi}, n=532; *ASNS*^{lo}, n=58); sunitinib (*ASNS*^{hi}, n=204; *ASNS*^{lo}, n=19). Middle line and whiskers represent the mean and the standard deviation respectively. One-sided Wilcoxon rank sum *P*-values are denoted for each drug. **f**, Volcano plot showing drug effectiveness in *ASNS*^{hi} cell lines as noted in panel **d**. Significance was evaluated using two-sided Wilcoxon rank sum test. Drugs inhibiting the

identified ASNS synthetic lethal partners are shown in blue. GW843682X, PLK1/3 inhibitor. **g**, Conditional essentiality of RTKs (*VEGFR-2* (*ASNS*^{hi}, n=37; *ASNS*^{lo}, n=38), *PDGFR-A* (*ASNS*^{hi}, n=69; *ASNS*^{lo}, n=67), and *PDGFR-B* (*ASNS*^{hi}, n=69; *ASNS*^{lo}, n=67)) and MAPK signaling pathway genes *BRAF* (*ASNS*^{hi}, n=80; *ASNS*^{lo}, n=74), *MEK1*(*ASNS*^{hi}, n=69; *ASNS*^{lo}, n=67), *ERK2* (*ASNS*^{hi}, n=35; *ASNS*^{lo}, n=40), *P90RSK1* (*ASNS*^{hi}, n=69; *ASNS*^{lo}, n=67), and *MNK1* (*ASNS*^{hi}, n=69; *ASNS*^{lo}, n=67)) in *ASNS*^{hi} and *ASNS*^{lo} cell lines. One-sided Wilcoxon rank sum *P*-values are denoted for each gene knockdown. In the boxplots, the top and bottom horizontal lines represent the 75th and the 25th percentile, respectively, and the middle horizontal line represents the median. The size of the box in boxplots represents the interquartile range, and the top and bottom whiskers represent the maximum and the minimum values respectively.

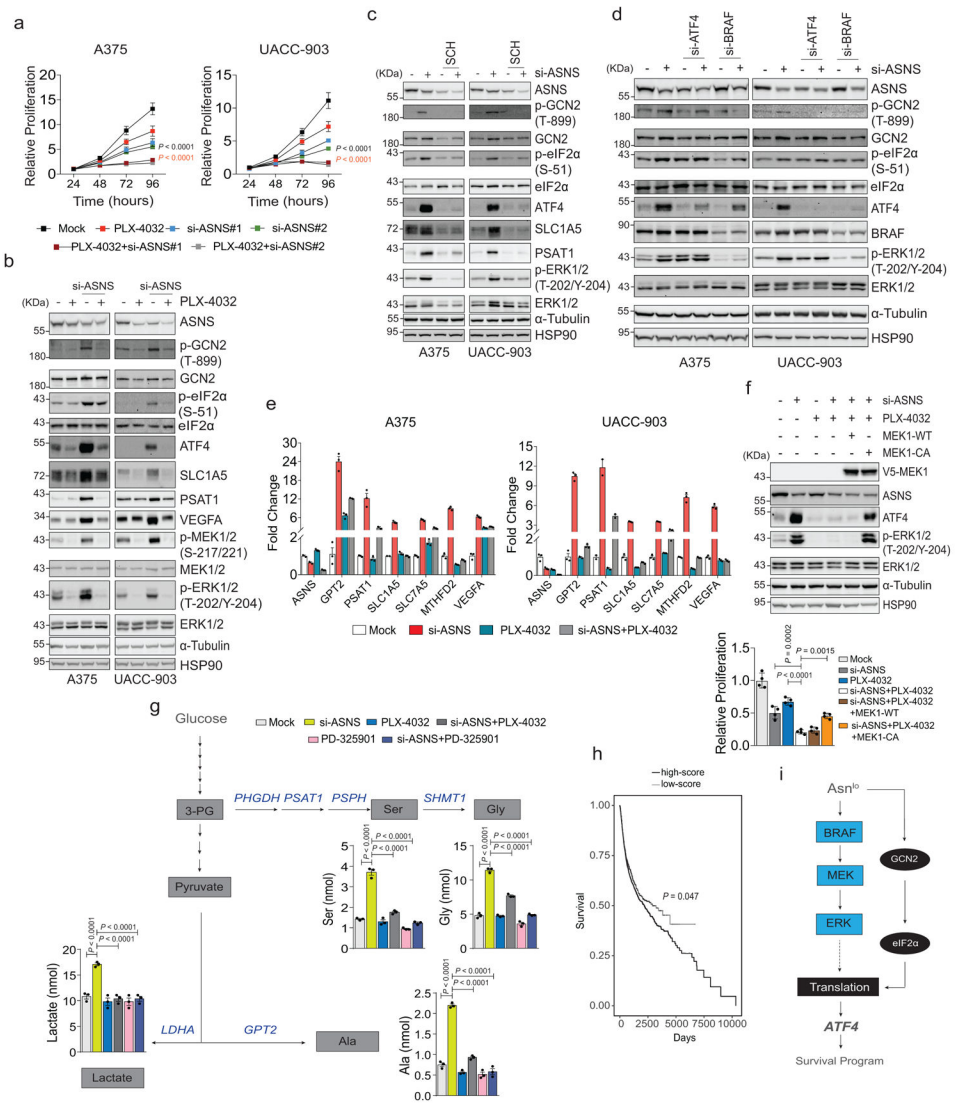

Fig. 3: The MAPK Pathway is Required for ATF4 Upregulation Upon Asparagine Limitation.

a, Proliferation of melanoma cells over indicated times following treatment with si-*ASNS*, BRAF-i (PLX-4032), or both relative to mock (NT-siRNA+DMSO). **b**, Immunoblotting of AAR pathway, VEGFA, and MAPK signaling components in melanoma cells 72 hr after treatment with si-*ASNS*, PLX-4032, or both. **c**, Immunoblotting of ASNS, AAR pathway and indicated proteins in melanoma cells 72 hr after treatment with si-*ASNS*, an ERK inhibitor (SCH-772984 (SCH)), or both. **d**, Immunoblotting of AAR pathway and indicated proteins in melanoma cells 72 hr after treatment with si-*ASNS*, si-*ATF4*, si-*BRAF*, or indicated combinations. **e**, qRT-PCR analysis for transcripts encoding ATF4 targets in melanoma cells 48 hr after treatment with si-*ASNS*, PLX-4032, or both. **f**, Immunoblotting of indicated proteins (top) and proliferation of A375 cells 72 hr after treatment with the indicated combinations (bottom). **g**, GC-MS-based estimation of intracellular amino acids levels in UACC-903 cells 72 hr after treatment with si-*ASNS*, PLX-4032, MEK-i (PD-325901), or indicated combinations. Scheme depicts the metabolites in the metabolic

cascade and the corresponding enzymes involved. **h**, Kaplan-Meier plot for patients with co-inactivation of *ASNS* and *BRAF* (grey; n=1,164) compared to the patients with active *ASNS* or *BRAF* (black; n=4,231; two-sided logrank P=0.047, ΔAUC=0.15) in pan-cancer analysis. **i**, Schematic showing regulation of ATF4 induction by MAPK signaling following asparagine suppression (Asn^{lo}). Data are representative of three experiments except **f**, representative of two independent experiments. Data are presented as the mean ± SEM of n=3 biological replicates in **a**, mean ± SEM of n=4 biological replicates in **f**, and mean ± SEM of n=3 technical replicates in **e.** Data presented as the mean ± SEM of n=3 independent experiments in **g**. Statistical significance was calculated using two-way Anova for **a**, two-tailed unpaired Student's t-test for **f**, and one-way Anova for **g**. In **a**, P-values in black and orange correspond to the comparison between si-*ASNS*#1 and si-*ASNS*#1+PLX-4032 and si-*ASNS*#2 and si-*ASNS*#2+PLX-4032 respectively.

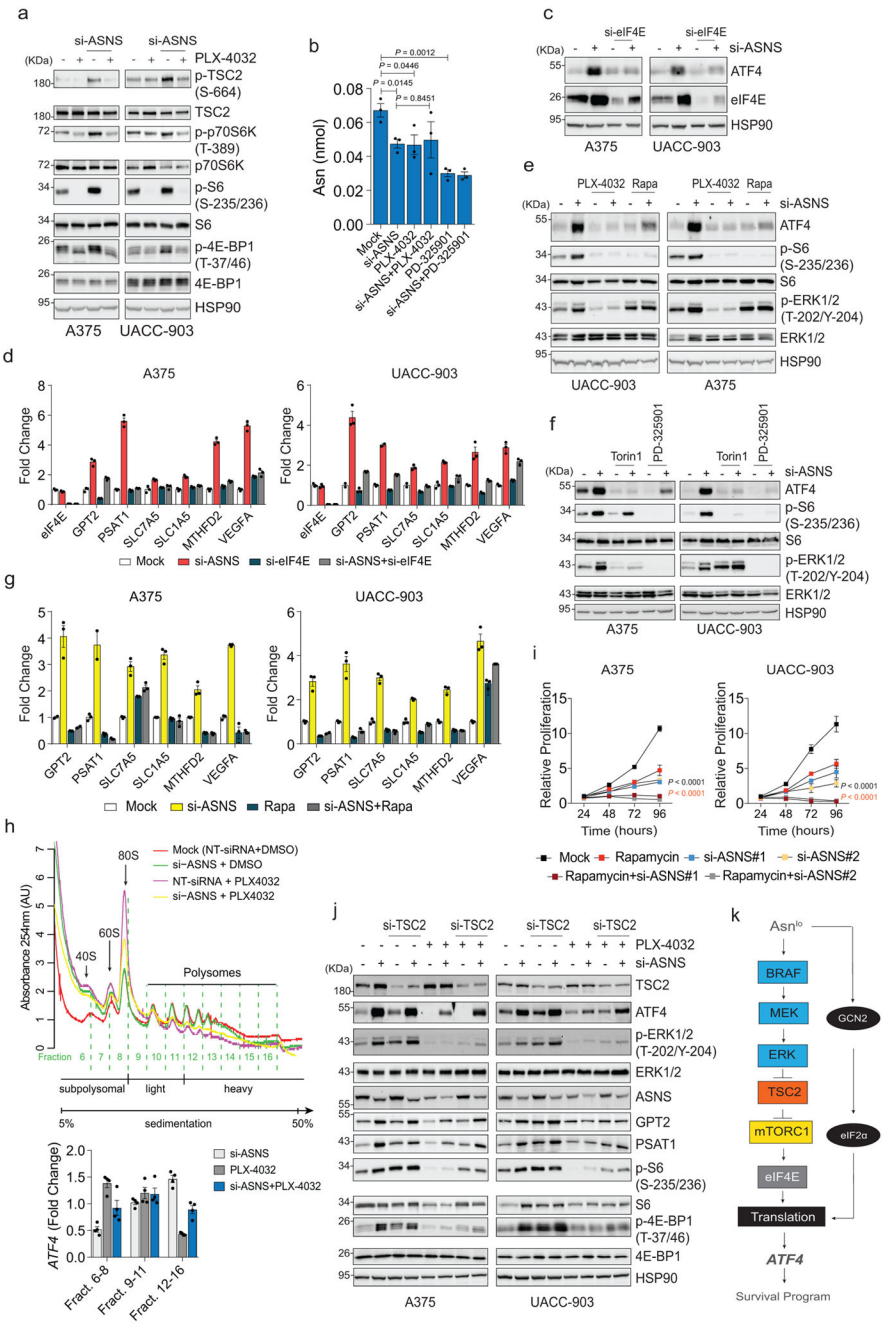

Fig. 4: ATF4 Induction Following ASNS Suppression requires MAPK-mTORC1-eIF4E Signaling.

a, Immunoblotting of indicated proteins in melanoma cells 72 hr after treatment with si-*ASNS*, PLX-4032, or both. **b**, GC-MS-based estimation of intracellular asparagine levels in UACC-903 cells treated as indicated for 72 hr. **c**, Immunoblotting of ATF4 and eIF4E in melanoma cells treated 72 hr with si-*ASNS*, si-*eIF4E*, or both. **d**, qRT-PCR analysis of transcripts encoding ATF4 targets in melanoma cells 48 hr after treatment with si-*ASNS*, si-*eIF4E*, or both. **e**, Immunoblotting of indicated proteins in melanoma cells 72 hr following indicated treatments. **f**, Immunoblotting of indicated proteins in melanoma cells 72 hr

following indicated treatments. **g**, qRT-PCR analysis of transcripts encoding ATF4 targets in melanoma cells 48 hr after treatment with si-*ASNS*, rapamycin, or both. **h**, Absorbance profiles at 254nm of A375 cells treated with si-*ASNS*, PLX-4032, or both for 48 hr (top), and qRT-PCR analysis of *ATF4* mRNA levels in subpolysomal, light, and heavy polysomal fractions of A375 cells treated with si-*ASNS*, PLX-4032, or both (bottom). Levels of mRNA are shown as fold-change relative to mock (NT-siRNA+DMSO); value set to 1.0. **i**, Proliferation of melanoma cells over indicated times following indicated treatments. **j**, Immunoblotting of indicated proteins in melanoma cells 72 hr after indicated treatments. **k**, Scheme depicting MAPK regulation of mTORC1 activity and consequent ATF4 translation; low asparagine levels (Asn^{lo}). Data are representative of three experiments and presented as the mean ± SEM of n=3 experiments in **b,** mean ± SEM of n=3 technical replicates in **d** and **g**, mean ± SEM of n=4 technical replicates in **h**, and mean ± SEM of n=3 biological replicates in **i**. Statistical significance was calculated using two-tailed unpaired Student's *t*-test except for **b** and two-way Anova for **i**. In **i**, *P*-values in black and orange correspond to the comparison between si-*ASNS*#1 and si-*ASNS*#1+rapamycin and si-*ASNS*#2 and si-*ASNS*#2+rapamycin respectively.

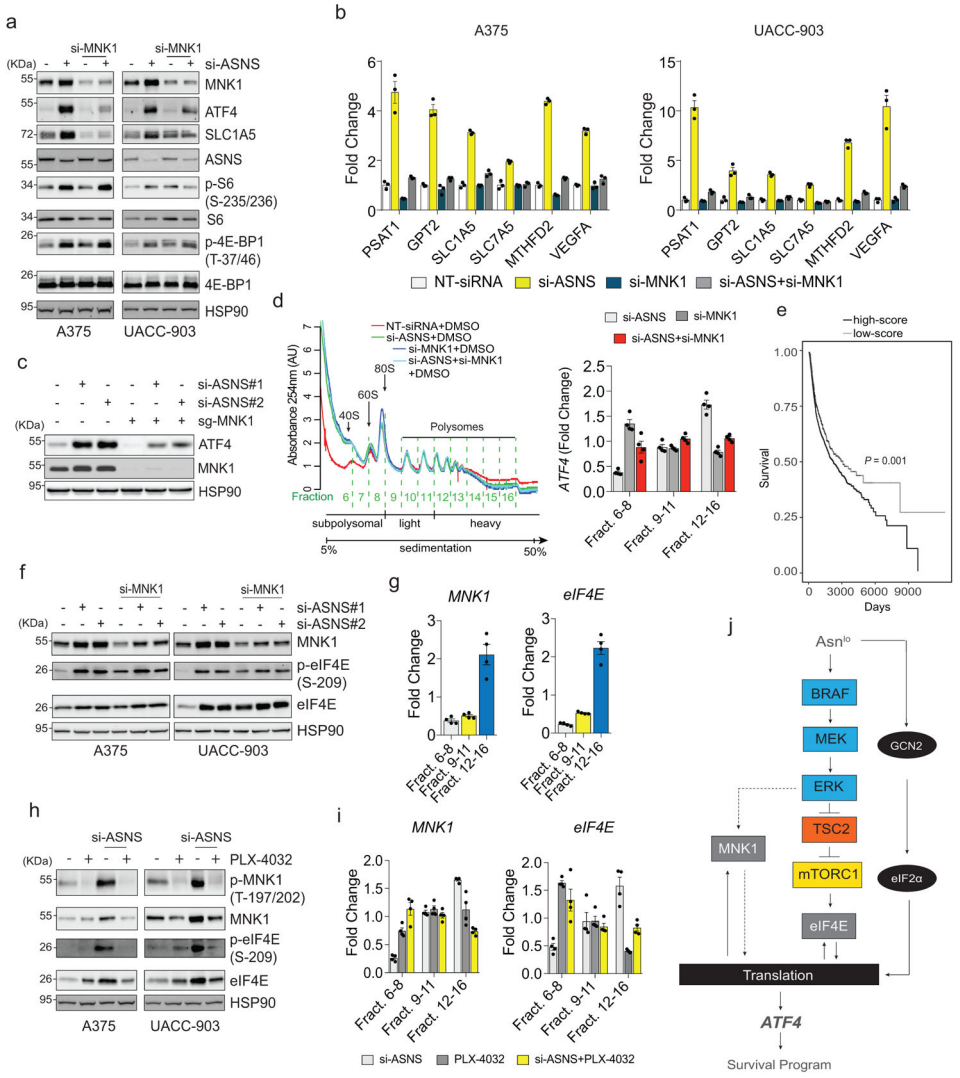

Fig. 5: MNK1 is Essential for ATF4 Induction in Response to Asparagine Limitation.

a, Immunoblotting of indicated proteins in melanoma cells 72 hr after treatment with si-*ASNS*, si-*MNK1*, or both. **b**, qRT-PCR analysis of transcripts encoding ATF4 targets in melanoma cells 48 hr after treatment with si-*ASNS*, si-*MNK1*, or both. **c**, Immunoblotting of ATF4 and MNK1 in A375 cells stably transduced with mock (Cas9 alone (−)) or Cas9 and single guide RNA (sgRNA) targeting MNK1 (sgMNK1), and treated with si-*ASNS*#1 or #2 for 72 hr. **d**, Absorbance profiles at 254nm of A375 cells treated with si-*ASNS*, si-*MNK1*, or both for 48 hr (left), and corresponding qRT-PCR analysis of *ATF4* mRNA levels in subpolysomal, light, and heavy polysomal fractions (right). Levels of mRNA shown as fold change in comparison to mock (NT-siRNA+DMSO). **e**, Kaplan-Meier plot shows the patients with co-inactivation of *ASNS* and *MNK1* exhibit better prognosis (grey; n=1,164) compared to the patients with active *ASNS* or *MNK1* (black; n=4,231; two-sided logrank P=0.001, ΔAUC=0.13) in pan-cancer analysis. **f**, Immunoblotting of indicated proteins in melanoma cells 72 hr after indicated treatments. **g**, qRT-PCR analysis of *MNK1* and *eIF4E* mRNA levels in subpolysomal, light, and heavy polysomal fractions of A375 cells treated

for 48 hr with si-*ASNS* relative to mock treatment. **h**, Immunoblotting of phospho and total MNK1 and eIF4E proteins in melanoma cells treated 72 hr with si-*ASNS*, PLX-4032, or both. **i**, qRT-PCR analysis of *MNK1* and *eIF4E* mRNA levels in subpolysomal, light, and heavy polysomal fractions of A375 cells treated for 48 hr with si-*ASNS*, PLX-4032, or both relative to mock treatment. **j**, Model showing regulation of ATF4 and associated survival mechanisms in asparagine-restricted cells; low asparagine levels (Asn^{lo}). Data are representative of three experiments and presented as the mean ± SEM of n=3 technical replicates in **b**, and mean ± SEM of n=4 technical replicates in **d**, **g**, and **i**.

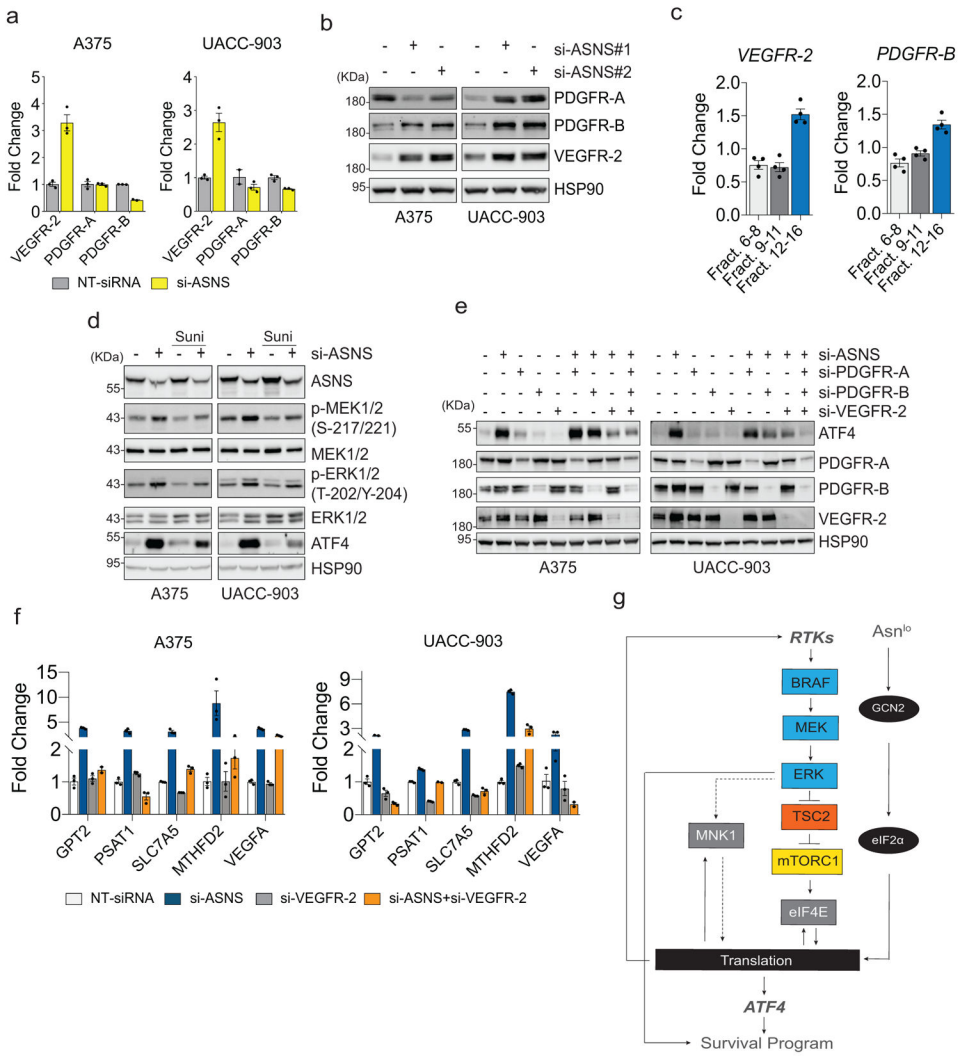

Fig. 6: ASNS Suppression Upregulates RTKs to Induce MAPK Signaling.

a, qRT-PCR analysis of transcripts encoding indicated RTKs in melanoma cells 48 hr after treatment with si-*ASNS*. **b**, Immunoblotting of VEGFR-2, PDGFR-A, and PDGFR-B in melanoma cells 72 hr after treatment with the indicated si-*ASNS*. **c**, qRT-PCR analysis of *VEGFR-2* and *PDGFR-B* mRNA levels in subpolysomal, light, and heavy polysomal fractions of A375 cells treated for 48 hr with si-*ASNS* relative to mock treatment. **d**, Immunoblotting of ASNS, ATF4, and phospho and total MEK1/2 and ERK1/2 proteins in melanoma cells 72 hr after treatment with si-*ASNS*, Sunitinib (Suni), or both. **e**, Immunoblotting of the indicated proteins in melanoma cells 72 hr after treatment with si-*ASNS*, si-*PDGFR-A*, si-*PDGFR-B*, si-*VEGFR-2*, or the indicated combinations. **f**, qRT-PCR analysis of transcripts encoding ATF4 targets in melanoma cells 48 hr after treatment with si-*ASNS*, si-*VEGFR-2*, or both. **g**, Model depicting cellular survival program orchestrated by translational reprogramming following suppression of asparagine levels (Asn^{lo}). Enhanced GCN2-eIF2α signaling promotes translational reprogramming, upregulating the expression of ATF4 and the components of translation initiation MNK1 and eIF4E, which are crucial for ATF4 translational induction. Altered translation also activates

RTK-MEK-ERK signaling, which impinges upon the translation initiation machinery to crucially regulate ATF4 translational enhancement, thus supporting a feed-forward loop to amplify survival signaling. Data are representative of three independent experiments and presented as the mean ± SEM of n=3 technical replicates in **a** and **f**, and mean ± SEM of n=4 technical replicates in **c**.

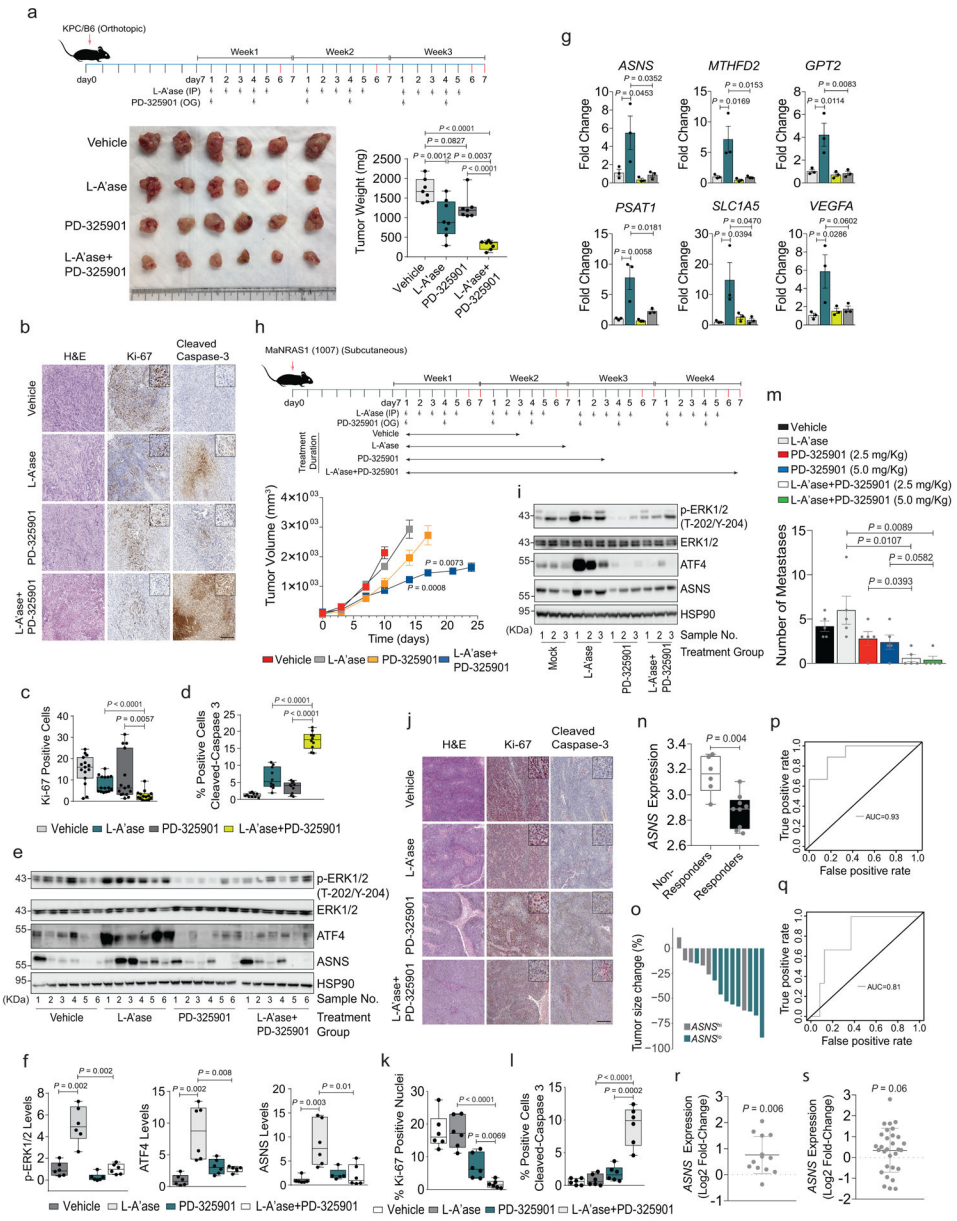

Fig. 7: Combined L-Asparaginase Treatment and MEK Inhibition Suppresses Pancreatic and Melanoma Tumor Growth.

a, Schematic showing the drug treatment regimen (top). Size (left) and weight (right) of KPC/B6 pancreatic tumors. Mice treated as indicated with vehicle (n=7), L-A'ase (n=8), PD-325901 (n=7), or a combination of L-A'ase and PD-325901 (n=7). IP, intraperitoneal; OG, oral gavage. Statistical analysis: one-way Anova. **b-d**, Representative images of H&E, Ki-67, and cleaved caspase-3 staining from each treatment group in **a** (**b**). Quantification of Ki-67 (**c**; n=15, each 15 fields) and cleaved caspase-3 (**d**; n=10, each 10 fields). Scale bar, 300 μm. **e**, Immunoblotting of resected pancreatic tumors (n=6 mice per group) for indicated proteins. **f**, Quantification of protein levels in **e**. **g**, qRT-PCR analysis of transcripts encoding ATF4 targets in resected pancreatic tumors (n=3 mice per group). **h**, (top) Schematic showing the drug treatment regimen. (bottom) Volume of tumors from C57BL/6 mice

injected subcutaneously with MaNRAS1 (1007) mouse melanoma cells and treated as indicated (n=8 mice per group). Statistical analysis: Welch's t-test (two-tailed). **i**, Immunoblotting of resected melanoma tumors (n=3 mice per group) for indicated proteins. Lysates from tumors harvested at timepoints indicated in **h**. **j-l**, Representative images of H&E, Ki-67, and cleaved caspase-3 staining from treatment groups in **h** (**j**). Quantification of Ki-67 (**k**; n=6, each 6 fields) and cleaved caspase-3 (**l**; n=6, each 6 fields). Scale bar, 300 μm. **m**, Number of lung metastasis from SW1 melanoma cells inoculated in C3H/HeN mice and subjected to indicated treatments (n=5 mice per group). Statistical analysis: two-tailed unpaired Student's t-test. **n**, Relative *ASNS* expression in melanoma patients treated with a BRAF or BRAF and MEK inhibitor(s) (non-responders, n=6; responders, n= 9). P-value calculated by one-sided Wilcoxon rank sum test. **o**, Waterfall plot for tumor size in patients treated as in **n**; patients were segregated based on high ($ASNS^{hi}$, n=6) and low ($ASNS^{lo}$, n=9) *ASNS* expression partitioned by the mean *ASNS* expression. **p**, **q**, Receiver-operating characteristics (ROC) analysis for predicted melanoma patient response to MAPK inhibitors based on *ASNS* expression in cohort 1 (**p**; AUC=0.93; responders n=9 and non-responders n=6) and cohort 2 (**q**; AUC=0.81; responders n=3 and non-responders n=24). **r**, **s**, Expression fold-change of *ASNS* between (**r**) post-treatment (BRAF-i or BRAF-i+MEK-i) and pre-treatment (n=13), or (**s**) post-treatment (BRAF-i) and pre-treatment (n=30) melanoma patient tumors (y-axis). Each dot represents a patient tumor sample. Middle line and whiskers represent the mean and the standard deviation, respectively. The P-value of paired Wilcoxon test following the adjustment multiple hypothesis correction (FDR) are displayed. Statistical significance was calculated using one-way Anova for **g** or two-tailed unpaired Student's t-test, unless specified. For MAPK pathway inhibitor treatments in (**n-q**) refer to Methods. Data information: In the boxplots, the top and bottom horizontal lines represent the 75th and the 25th percentile, respectively, and the middle horizontal line represents the median. The size of the box represents the interquartile range, and the top and bottom whiskers represent the maximum and the minimum values respectively.